

Review

A Review on the Overall Performance of Metal Hydride-Based Hydrogen Storage Systems

Puchanee Larpruenrudee ¹, Nick S. Bennett ¹, Zhen Luo ¹, M. J. Hossain ², Nawshad Haque ³, Emilie Sauret ⁴, Robert Fitch ¹ and Mohammad S. Islam ^{1,*}

¹ School of Mechanical and Mechatronic Engineering, University of Technology Sydney, Ultimo, NSW 2007, Australia; puchanee.larpruenrudee@uts.edu.au (P.L.); nicholas.bennett@uts.edu.au (N.S.B.); zhen.luo@uts.edu.au (Z.L.); robert.fitch@uts.edu.au (R.F.)

² School of Electrical and Data Engineering, University of Technology Sydney, 15 Broadway, Ultimo, NSW 2007, Australia; jahangir.hossain@uts.edu.au

³ CSIRO Mineral Resources, Clayton South, Melbourne, VIC 3169, Australia; nawshad.haque@csiro.au

⁴ School of Mechanical, Medical and Process Engineering, Faculty of Engineering, Queensland University of Technology, Brisbane, QLD 4000, Australia; emilie.sauret@qut.edu.au

* Correspondence: mohammadsaidul.islam@uts.edu.au

Abstract: Metal hydride-based hydrogen storage (MHHS) has been used for several purposes, including mobile and stationary applications. In general, the overall MHHS performance for both applications depends on three main factors, which are the appropriate selection of metal hydride material uses, design configurations of the MHHS based on the heat exchanger, and overall operating conditions. However, there are different specific requirements for the two applications. The weight of the overall MHHS is the key requirement for mobile applications, while hydrogen storage capacity is the key requirement for stationary applications. Based on these requirements, several techniques have been recently used to enhance MHHS performance by mostly considering the faster hydrogen absorption/desorption reaction. Considering metal hydride (MH) materials, their low thermal conductivity significantly impacts the hydrogen absorption/desorption reaction. For this purpose, a comprehensive understanding of these three main factors and the hydrogen absorption/desorption reaction is critical and it should be up to date to obtain the suitable MHHS performance for all related applications. Therefore, this article reviews the key techniques, which have recently been applied for the enhancement of MHHS performance. In the review, it is demonstrated that the design and layout of the heat exchanger greatly affect the performance of the internal heat exchanger. The initial temperature of the heat transfer fluid and hydrogen supply pressure are the main parameters to increase the hydrogen sorption rate and specific heating power. The higher supply pressure results in the improvement in specific heating power. For the metal hydride material selection under the consideration of mobile applications and stationary applications, it is important to strike trade-offs between hydrogen storage capacity, weight, material cost, and effective thermal conductivity.

Keywords: metal hydride; hydrogen storage; hydrogen absorption and desorption; thermal design; heat transfer enhancement; heat exchanger



Academic Editor: Nikolaos Koukouzas

Received: 14 February 2025

Revised: 25 February 2025

Accepted: 3 March 2025

Published: 6 March 2025

Citation: Larpruenrudee, P.; Bennett, N.S.; Luo, Z.; Hossain, M.J.; Haque, N.; Sauret, E.; Fitch, R.; Islam, M.S. A Review on the Overall Performance of Metal Hydride-Based Hydrogen Storage Systems. *Energies* **2025**, *18*, 1291. <https://doi.org/10.3390/en18051291>

Copyright: © 2025 by the authors. Licensee MDPI, Basel, Switzerland. This article is an open access article distributed under the terms and conditions of the Creative Commons Attribution (CC BY) license (<https://creativecommons.org/licenses/by/4.0/>).

1. Introduction

Thermal energy storage techniques store hydrogen for the purpose of producing electricity. Hydrogen has been proposed as the most promising energy carrier to store renewable energy for both stationary and mobile applications. Under hydrogen storage

in stationary applications, these include stationary power generation, on-site storage for utilisation, and on-site storage for production. For hydrogen storage in mobile applications, these include hydrogen transportation and vehicle fuel, such as automotive, aerospace, and maritime industries.

The main advantages of hydrogen for energy storage are its characteristics and portability and its ability to offer high energy capacity per unit mass, which is significantly higher than that of fossil fuels [1]. For this purpose, hydrogen energy storage has been applied for both small-scale and large-scale applications. Focusing on the high demand for hydrogen, underground hydrogen storage is one of the suitable options as this storage offers a large volume to store hydrogen with several options such as deep aquifers, salt caverns, depleted deposits of natural gas and oil, and others [2].

The recent advancement in subsurface hydrogen farming significantly highlights the importance of biotic and abiotic processes to convert the indigenous components, gases, and nutrients into hydrogen [3]. To prevent leakage and ensure efficient hydrogen production, stability of surrounding geological materials is required [4]. Furthermore, clay minerals also can withstand the conditions required for subsurface hydrogen generation. This greatly supports the development of safe and effective hydrogen production technologies [4]. To meet the demand, large amounts of hydrogen must be safely stored at low costs.

In general, hydrogen energy storage can be classified into three main types, which are compressed gas, liquid storage, and solid / material-based storage. For the first method, hydrogen is stored by compression into a selected container, such as steel and carbon fibre cylinders. Liquid storage is also another type of hydrogen storage. Using this technique, hydrogen can be stored in a liquid state at ambient temperature [5]. Compared to other storage types, solid storage requires lesser energy consumption and less operating time [6]. Therefore, storing hydrogen in solid form is the most efficient technique that has been widely used around the world.

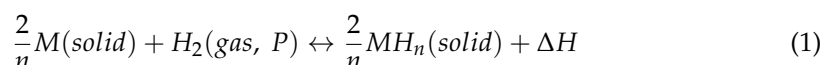
In regard to solid storage, this technique includes metal hydrides, complex hydrides, chemical hydrides, and adsorbents.

- Complex hydrides and chemical hydrides: These two techniques are primarily used to store hydrogen by absorption. However, the main problems of these techniques are the lack of reversibility and the complexity of the reaction process to extract hydrogen [2].
- Adsorbents: Porous materials are employed to absorb hydrogen. This technique provides better thermal management in the charging and discharging processes than other three techniques, including metal hydride, chemical hydride, and complex hydride [7]. However, this technique negatively affects storage capacity when focusing on large-scale commercialisation [8].
- Metal hydride: Metal hydride (MH) has recently attracted significant interest as it offers high hydrogen capacity, low material cost for storage applications, and high safety performance [8–11].

Figure 1 presents the different technologies of hydrogen storage that have been widely used in various fields.

Basically, metal hydrides are powders. When metal powders absorb hydrogen to form hydrides, heat is released. When hydrogen is released from a hydride, heat is absorbed instead. The processes are provided in Figure 2.

The hydrogen reaction for absorption and desorption is generally expressed as



In general, it is the chemical reaction between metal alloys and hydrogen. Hydrogen can be stored or released from the storage by absorption and desorption processes. This

chemical reaction is reversible as it is the exothermic reaction for hydrogen absorption and the endothermic reaction for hydrogen desorption (from Equation (1)).

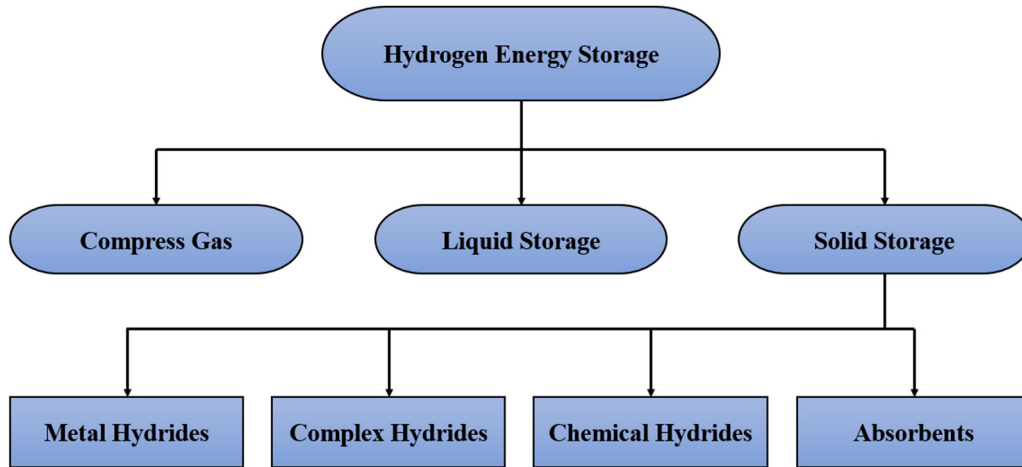


Figure 1. Different technologies of hydrogen energy storage.

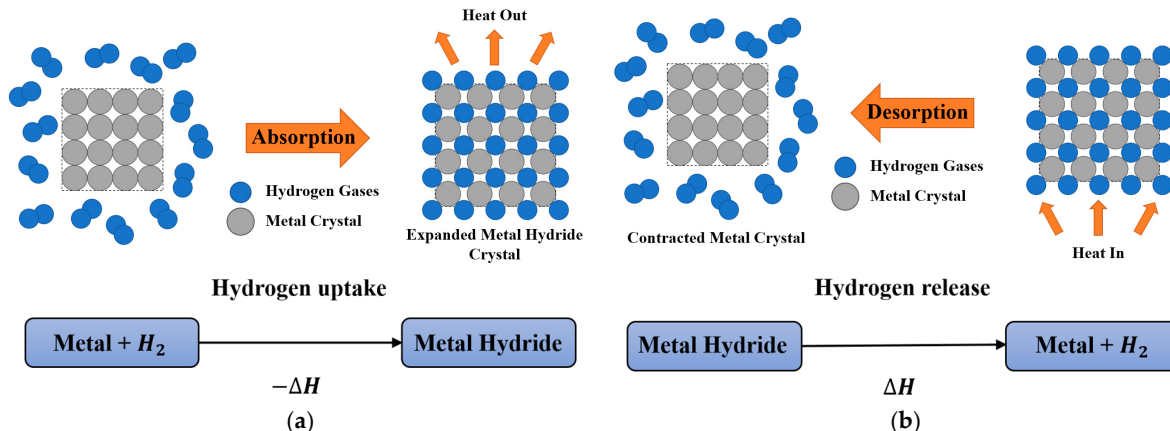


Figure 2. Absorption and desorption processes of metal hydride; (a) hydrogen absorption process and (b) hydrogen desorption process.

The amount of hydrogen (X) that is absorbed and desorbed on a metal surface can be expressed in weight percentage (wt%). The rate of this sorption is associated with reaction kinetics according to the following equations.

For hydrogen absorption [12]:

$$\frac{dX}{dt} = C_a \cdot \exp\left(\frac{-E_a}{RT}\right) \cdot \left(\frac{P_{H_2} - P_{eq}}{P_{eq}} \right) \cdot (X_{max} - X) \quad (2)$$

where C_a denotes the absorption rate constant and E_a refers to the activation energy for hydrogen absorption. P_{H_2} is the hydrogen supply pressure. X_{max} is the maximum amount of hydrogen which is considered to be one for the full amount of hydrogen reaction fraction. The current amount of hydrogen in reaction fraction term (X) ranges from 0 to 1.

For hydrogen desorption [12],

$$\frac{dX}{dt} = C_d \cdot \exp\left(\frac{-E_d}{RT}\right) \cdot \left(\frac{P_{H_2} - P_{eq}}{P_{eq}} \right) \cdot (X) \quad (3)$$

where C_d is the desorption rate constant and E_d is the activation energy for hydrogen desorption.

The equilibrium pressure (P_{eq}) inside the MH storage for absorption and desorption can be determined by using Van't Hoff equation as follows [13]:

$$\ln \frac{P_{eq}}{P_{ref}} = \frac{\Delta H}{RT} - \frac{\Delta S}{R} \quad (4)$$

where P_{ref} is the reference pressure. ΔH and ΔS are the enthalpy of reaction and entropy of reaction, respectively. R refers to the universal gas constant.

The hydrogen reaction kinetics (refer to Equations (2) and (3)) are mainly influenced by the heat transfer rate inside the storage system as the limitation of MH performance is the slow reaction kinetics to absorb and desorb the hydrogen due to a low thermal conductivity of MH material [14]. This mainly affects the overall metal hydride-based hydrogen storage (MHHS) performance. Therefore, the design optimisation of MHHS under various techniques has been considered for the improvement in MHHS performance.

One of the most effective methods to enhance the overall MHHS performance is appropriate thermal management to control the hydrogen flow rate during absorption and desorption [15]. This significantly improves the hydrogen reaction kinetics. A faster MH bed temperature reduction leads to faster hydrogen absorption. In contrast, a higher MH bed temperature is required for the hydrogen desorption process. The enhancement of heat transfer performance techniques has been used to fulfil this limitation based on the design and optimisation of heat exchangers. Not only the development of these heat exchangers but also the overall MHHS performance is affected by other factors. In general, the overall MHHS performance for each specific application is dependent on three main factors. Appropriately selecting the overall operating conditions, material uses, and design configurations of the MHHS based on heat exchangers are essential requirements as these factors can positively or negatively affect the overall system performance, such as the volumetric and gravimetric properties of the storage system and the hydrogen reaction kinetic.

Considering storage applications, there are different requirements of the MHHS configurations between the MHHS for mobile applications and the MHHS for stationary applications. The weight of the overall MHHS is the key factor for mobile applications, while the hydrogen storage capacity is the key factor for the MHHS in stationary applications. However, both storage applications also require superior hydrogen reaction kinetics to store and release hydrogen when it is needed. For these purposes, comprehensive understanding of these three factors (operating condition, material uses, and heat exchanger design configurations) and hydrogen reaction kinetics on the overall MHHS performance for both mobile and stationary applications should be prioritised and up to date. Therefore, the main objective of this paper is to review the current trends in the use of MH materials, heat exchanger design configurations, as well as the selected parameters for operating conditions by considering the effect of these factors on the hydrogen reaction kinetics under the overall requirement of the MHHS for both mobile and stationary applications. The MH materials are reviewed under heat transfer performance, cost, density, and their effect on the overall MHHS performance for both mobile and stationary applications. The design and optimisation of heat exchangers, choice of heat transfer fluids (HTFs), and operation parameters are considered as the key techniques to improve the reaction kinetic, resulting in the enhancement of the overall MHHS performance. The heat exchanger configurations based on thermal management methods, including active and passive methods, are considered in this article under both inner and outer heat exchanger structures that affect the hydrogen absorption/desorption reaction and overall volumetric/gravimetric of the MHHS. In addition, the operating conditions for the MHHS and the HTF are analysed by

focusing on the hydrogen absorption/desorption duration and its improvement under the different MHHS configurations.

2. Metal Hydride Materials

The main component of MHHS is the MH material. An appropriate selection of MH material is one of the most important parameters that can significantly impact overall MHHS performance for both mobile and stationary applications. Different metal alloys have different thermo-physical properties that influence hydrogen absorption/desorption, storage capacity, etc. Metal alloys should offer high hydrogen storage capacity and high thermal conductivity, fast reaction kinetics, short refuelling time, low cost, easy availability, and high cyclic stability [16]. The low gravimetric density of the MH material is important for automobile applications as the size of the MHHS and the vehicle must be suitable to provide an appropriate driving range. In contrast, the high volumetric density of MH is required for stationary applications as the weight of the overall storage system does not affect storage efficiency [17].

This section summarises the main characteristics of MH materials that affect the overall MHHS performance for both mobile and stationary applications. These include hydrogen storage capacity, effective thermal conductivity, density, and raw cost materials. Under the MH material sections, several techniques have been widely used to study MH materials and their properties, such as experimental works and numerical works based on the computational fluid dynamics (CFDs) method and the machine learning method.

2.1. Machine Learning Techniques for Investigation of Metal Hydride Material Properties

In general, machine learning (ML) is used to predict future outcomes based on previous data which can be obtained from different sources such as the CFD method and experimental works [18,19]. A large dataset is the first requirement for training of the ML technique. Then, the appropriate selection of related parameters (descriptors) is the key factor for the ML algorithm to efficiently learn from previous data and then predict an accurate outcome [20]. Some studies also use ML to analyse and predict the thermal performance of pin fin heat exchangers by considering several related parameters. These include the fin space, thickness, material, and conductive heat transfer coefficient [21–26]. For the development of hydrogen technologies, ML has been used to predict the results in various applications, including hydrogen production [27,28], hydrogen storage [29,30], and hydrogen conversion in fuel cells [31,32]. In recent years, ML has become well known as a useful method for analysing MH databases to classify the materials' uses and their properties as these factors play an important role in the requirement of MHHS properties [33].

Several models for ML methods have been applied to hydrogen applications, especially to the MHHS. A study by Rahnama et al. [34] employed ML to predict hydrogen storage capacity in weight percentage and identify the most conducive MH material for efficient r fuel cell application. The database based on more than 1600 references was collected from the International Energy Agency Hydrogen Implementing Agreement that was funded by the U.S. Department of Energy (<https://www.energy.gov/eere/fuelcells/databases>, accessed on 6 November 2024). The MH classes from the database included Mg alloys (373 samples), complex hydrides (234 samples), solid solution alloys (263 samples), AB (179 samples), A₂B (140 samples), AB₂ (625 samples), AB₅ (477 samples), and Misc intermetallic compounds (431 samples). For hydrogen weight percentage, correlations were made based on the relationship between hydrogen weight percentage, temperature, heat formation, material class, composition formulas, and pressure. The results from these studies proved that the ML-boosted decision tree algorithm obtained the best performance with a 0.83 of coefficient of determination compared to other models, including Bayesian linear

(0.56), neural network (0.60), and linear regression (0.50). However, for the classification of materials used by considering the heat of formation and hydrogen content, the neural network provided better performance for obtaining hydrogen weight percentage with a 0.80 accuracy compared to logistic regression (0.47 accuracy), decision forest (0.60 accuracy), and decision jungle algorithms (0.62 accuracy). Withman et al. [30] also employed a similar database to analyse the relationship between the alloys and MH properties. The results from Withman et al. [30] showed that the molecular volume of alloys is the most important factor for thermodynamic predictors. This finding also supported the results from other previous studies [35–37]. However, the database from HydPARK (refer to U.S. Department of Energy) contained data from the previous study and only up to 2004. Therefore, the recent study from Suwarno et al. [33] was based on the database of AB₂-based MH classes from 1998 to 2019. The 314 pairs of AB₂ alloys were taken with their own hydrogen storage properties, including heat formation, phase abundance, and hydrogen storage capacity. This study proved that Ni, Cr, and Mn significantly affected the hydrogen properties, while only the Cr element significantly influenced the phase fraction (refer to phase abundance). The uses of ML for MH property prediction and their accuracy outcomes are summarised in Figure 3 and Table 1.

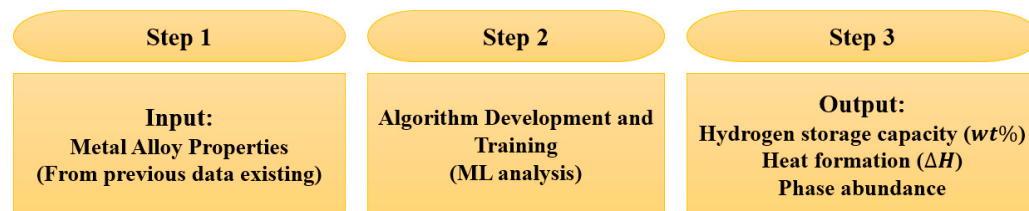


Figure 3. Machine learning techniques for metal hydride property prediction.

Table 1. Comparison of a coefficient of determination (R^2) between various machine learning algorithms for different parameters of AB₂-based MH properties.

ML Algorithms	Coefficient of Determination (R^2)			Reference
	Hydrogen Storage Capacity (in wt%)	Phase Abundance	Heat Formation	
Multivariate regression	0.667	0.448	0.367	
Decision tree	0.498	0.785	0.346	[33]
Random forest	0.688	0.832	0.647	
Boosted decision tree regression	0.830	-	-	
Baysian linear regression	0.569	-	-	
Neural network regression	0.608	-	-	[17,34]
Linear regression	0.502	-	-	

Note: It should be noted that the investigation of these factors is based on the actual dataset of hydrogen weight percentage, heat formation, operating temperature, and pressure.

It can be seen that the accuracy of predicted results is usually based on the selection of the ML algorithm. An appropriate selection of ML algorithms is required to obtain accurate results. However, the ML techniques are currently applied for the study of MH material properties only. Furthermore, these ML techniques are mainly used to analyse the hydrogen storage capacity of each MH material only. From these studies, hydrogen storage capacity, phase abundance, and heat formation are only considered under AB₂-based MH materials. Furthermore, the maximum hydrogen storage capacity under these studies is still lesser than 0.9 wt%.

2.2. Hydrogen Storage Capacity

According to the target of the American Department of Energy (DOE) [38], the hydrogen storage capacity (HSC) for commercialisation is expected to be at 6.5 wt% with a low decomposition temperature ranging from 60 to 120 °C. However, this target has still not been achieved as the metal alloys with low operating temperature usually obtain a low HSC of less than 2 wt%. In contrast, metal alloys with high HSC usually require a high operating temperature to activate the system. Table 2 summarises the operating condition ranges and the HSC of some commonly used metal alloys.

Table 2. Operating conditions and hydrogen capacity (wt%) of some commonly used metal alloys.

Metal Alloy	Operating Temperature (K)	Operating Pressure (MPa)	Hydrogen Capacity (wt%)	Reference
LaNi ₅	293	2.00	0.25	[39]
	0–373	5.00	1.44	[40]
	285	0.1	1.37	[41]
LaNi _{4.7} Al _{0.3}	193–413	0.00–6.00	1.43	[42]
Mg ₂ Ni	573	2.90	3.20	[43]
	573	1.16	3.50	[44]
	553	0.10–0.20	3.53	[45,46]
	553	0.10–1.50	4.10	[47]
	528	0.1	3.59	[41]
MmNi _{4.5} Al _{0.5}	298	0.38	1.2	[16]
NaAl	353–453	7.60–9.10	5.00	[44]
Ti _{1.1} CrMn	293	3.3	1.80	[48]
TiFe	298	0.41	1.86	[16]
TiMn _{1.5}	298	0.84	1.9	[16]

Several metal alloys have been developed to improve storage performance. Light metals, such as Li, Be, Na, Mg, B, and Al, are mainly used to form a large variety of MH compounds. Metal alloys can be classified into two main types: complex hydrides and intermetallic compounds. Complex hydrides are lightweight storage materials. Among other elements, sodium (Na), lithium (Li), and beryllium (Be) are the three elements that are lighter than magnesium and can be used as MH materials [9]. Sodium aluminium or NaAl-based alloys are two of the considerable choices as they obtain a high HSC, which is up to 5 wt%. However, the limitations of complex hydrides are kinetic and thermodynamic. Intermetallic compounds are widely used as MH materials as these alloys only require low temperature and pressure ranges for system activation that is close to ambient temperature (293 K or 20 °C) and pressure. Normally, these compounds are determined based on their crystal structures, such as AB₂, AB₅, and Ti-based body-centred cubic. Among intermetallic compounds, lanthanum nickel or LaNi₅-based alloys are the most popular alloys which have been recently used in several applications. However, the main problem of these alloys is the HSC with around 1.4 wt% at the maximum. The LaNi₅-based alloys and the storage capacity of other intermetallic compounds is also lesser than 2 wt%. Magnesium hydride is well known as a lightweight material for solid-state storage applications with a high storage capacity of 7.6 wt% [11,49,50]. However, it has slow kinetics and requires high temperature ranges for absorption and desorption. Therefore, several magnesium-based or Mg-based alloys have been developed for storage applications. The advantages of these alloys are high storage capacity, excellent heat resistivity, and good recyclability [11,51]. Among several Mg-based alloys, magnesium–nickel alloys (Mg₂Ni) have received much

more attention as they provide a considerable HSC of up to 6 wt% and faster reaction kinetics for hydrogen sorption compared to magnesium hydride [52]. However, these alloys still require a high temperature range to activate the system at around 523–603 K or 250–330 °C.

2.3. Effective Thermal Conductivity

Effective thermal conductivity (ETC) is the main parameter that directly affects the heat and mass transfer performance within the MH beds. In general, the main problem of the MHHS is the low ETC (between 0.1 W/mK and 1.5 W/mK) which leads to the slow heat transfer rate. This problem negatively affects hydrogen absorption and desorption. The operating conditions and ETC of some commonly used metal alloys are provided in Table 3.

Table 3. Operating conditions and effective thermal conductivity of some commonly used metal alloys.

Metal Alloy	Operating Temperature (K)	Operating Pressure (MPa)	Effective Thermal Conductivity (W/mK)	Reference
LaNi ₅	293–333	0–1.0	0.1–1.5	[53–55]
LaNi _{4.7} Al _{0.3}	253–413	0.0–6.0	0.1–1.1	[42]
Mg ₂ Ni	308–473 373	0.1–4.0 0.2–4.5	0.35–0.75 0.66–0.83	[56] [57]
MnNi _{4.5} Mn _{0.5}	313–333	0.1–3.0	0.7–1.3	[58]
MmNi _{4.5} Al _{0.5}	273–373	0–5.0	0.1–1.2	[59]
MmNi ₄ Fe	273	0.2–4.5	0.8–1.05	[57]
NaAl	303–473	0–5.0	0.25–1.2	[60–62]
Ti _{1.1} CrMn	293–300	0.3–25.3	0.3–0.7	[63]
TiFe	298	-	1.49	[64]
TiFe _{0.85} Mn _{0.15}	273–373	0–5.5	0.1–1.5	[65]
TiMn _{1.5}	294, 311	0.1–5.0	0.2–1.3	[66,67]

From Table 3, the maximum ETC from intermetallic compounds and complex hydrides (such as LaNi₅ and Ti-based alloys) is over 1 W/mK, while the maximum ETC from the magnesium–nickel-based alloys (Mg₂Ni) is lesser than 1 W/mK. However, most of them require a high operating temperature (over 333 K or 60 °C) to achieve the maximum ETC, except LaNi₅, MnNi_{4.5}Al_{0.5}, MmNi₄Fe, and TiFe alloys. Similarly, most metal alloys also require a high operating pressure to reach the maximum ETC, except the LaNi₅ alloy. The operating pressure range varies, but it is at least 0–3 MPa for most of them, except the LaNi₅ alloy, which requires only 0–1 MPa.

2.4. Density and Raw Cost Materials

The material's weight and raw cost materials are the main parameters for on-board hydrogen storage. Magnesium-based alloys are well known as lightweight and low-cost materials compared to other alloys. The summary of density and raw cost materials from some commonly used metal alloys are presented in Figures 4 and 5, respectively. In Figure 4, it can be seen that the density of the Mg₂Ni alloy is lower than that of other alloys as there is only 3.6 g/cc, while the density of the Ti-based alloy is over 6.4 g/cc. The density of mischmetal (Mm) alloys is over 8.1 g/cc, which is similar to LaNi₅ with 8.3 g/cc of density. However, the lanthanum–nickel alloy based on LaNi_{4.7}Al_{0.3} has 7.6 g/cc of density.

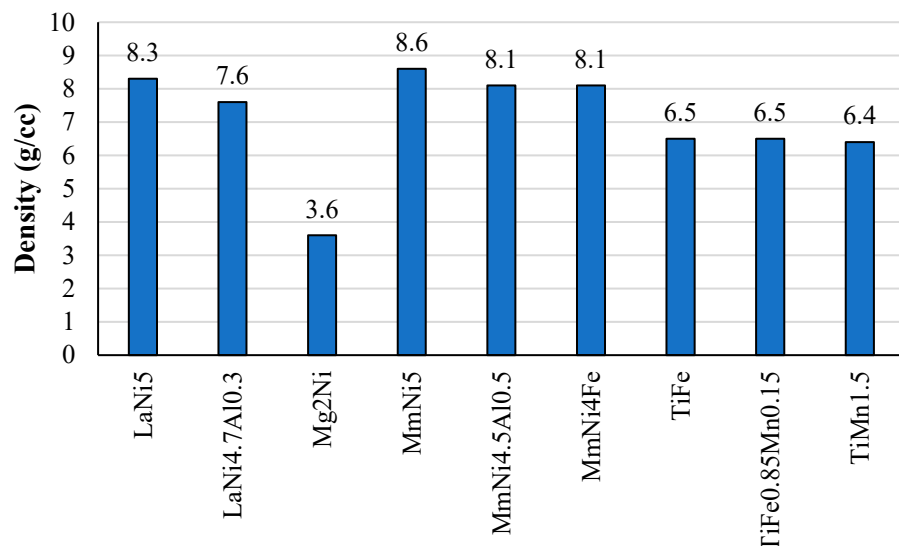


Figure 4. Comparison of density between some commonly used metal alloys [68].

From the available literature, the lanthanum–nickel-based alloys have the highest cost, which is over 9 USD/kg. Therefore, the cheaper element mixture, mischmetal (Mm), was used instead of lanthanum in the LaNi₅ alloy [69]. The raw cost reduces from 9 USD/kg to 7 USD/kg when using the Mm-based alloy instead of the La-based alloy. However, the cost is still higher than that of other alloys, especially the Mg-based and Ti-based alloys. The raw cost of Ti-based alloys is lower than that of other alloys as it is less than 5 USD/kg, while the raw cost of the Mg₂Ni alloy is 6.26 USD/kg. It should be noted that the raw material cost from the available literature in this article is from 1996, which was taken from the four references [69–72]. The cost of raw materials might be higher in the present.

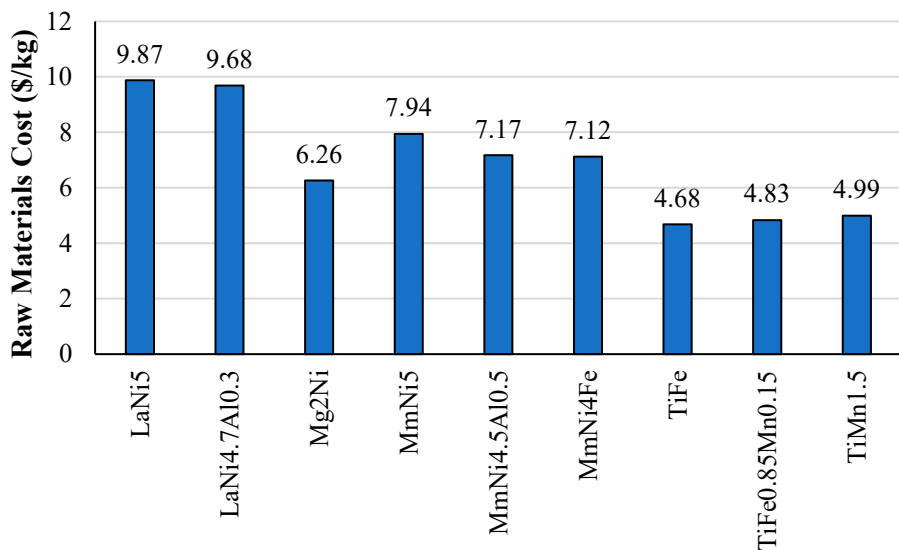


Figure 5. Comparison of raw materials cost between some commonly used metal alloys (price basis: mid-1996) [69–72].

From these comparisons (refer to Sections 2.2–2.4), magnesium-based metal alloys mostly have a high HSC, light weight, and low cost, but they have a low ETC. Intermetallic compounds, such as lanthanum nickel-based and titanium-based alloys, usually have a low HSC but they have a high ETC. Mischmetal-based alloys have a lower density and cost among intermetallic compounds than lanthanum nickel-based alloys. However, these alloys' density and raw material cost are still higher than those of titanium-based alloys.

Focusing on the material, the low-cost MH is also important for economic purposes. Most MH materials which offer a high HSC and light weight usually have a low ETC. In contrast, most MH materials which have a high ETC usually have a heavy weight and a low HSC. Therefore, the HSC and cost should be optimised while the ETC should be enhanced for MH materials. A low ETC negatively affects hydrogen reaction kinetics, resulting in a decrease in the overall MHHS performance. Considering the specific requirements of both small- and large-scale MHHS applications, magnesium-based metal alloys seem to be the most suitable MH material for both applications as these alloys offer a light weight for compact MHHS applications and a high HSC for large-scale MHHS applications. However, the slow hydrogen reaction kinetics rate due to the low ETC is the main problem of these alloys. One of the most effective ways to improve the hydrogen reaction kinetics rate is the enhancement of heat transfer performance inside the MHHS. This can be achieved by the design and optimisation of the heat exchanger configurations. Furthermore, the heat exchanger configurations should be designed with consideration of volumetric and gravimetric parameters of the overall MHHS.

3. Heat Exchanger Design Optimisation for Thermal Management

In general, the heat transfer limitation of the metal hydride materials is the main factor that limits MHHS performance. This is due to the strong dependence of absorption equilibrium pressure on temperature and low thermal conductivity of MH materials. This combination creates significant temperature gradients because of the exothermic nature of hydrogen absorption. This phenomenon results in the heat and mass transfer crisis as well as slow hydrogen absorption. Similarly, due to the endothermic nature of hydrogen desorption, heat is required to reverse the hydrogen absorption reaction. However, due to the low thermal conductivity of MH materials, the heat is not efficiently absorbed from the surroundings, leading to slow hydrogen desorption. Therefore, the heat exchanger configuration is one of the key factors to improve MHHS performance, as it significantly improves heat transfer performance inside the storage system.

Among MHHS studies from the 1990s and before 2020, 40% focused on experimental studies, while the rest focused on numerical studies [73]. Most recent works from 2020 still employed numerical simulation to perform studies by considering the design optimisation of heat exchanger configurations. Therefore, several heat exchanger configurations have been designed and optimised based on numerical simulations, especially the computational fluid dynamics (CFDs) method. Several designs for heat exchangers have been proposed and optimised for thermal management in active and passive methods. The improvement in heat transfer performance based on various heat exchanger types leads to the enhancement of hydrogen reaction kinetics, resulting in the enhancement of the overall MHHS performance. This section summarises the heat exchanger types under the active and passive methods that have been used for the MHHS on small and large scales.

The active heat exchanger design optimisations of the MHHS include an internal and an external heat exchanger, such as a cooling/heating tube and cooling/heating jacket. The schematic diagram of an MHHS with external and internal heat exchangers is provided in Figure 6. For both techniques, the HTF and hydrogen are injected from opposite directions during the absorption process as this increases the heat transfer rate compared to the case with injection in the same direction. The HTF is injected from the bottom part, while the hydrogen is injected from the top surface of the reactor. For external heat exchanger based on the cooling jacket, there is heat transfer between the outer MH bed as this area is directly close to the HTF which covers the area around the MHHS. The MHHS is cooled down starting from the outer MH bed area first. However, the MHHS is cooled down starting from the inner MH bed area first when the internal heat exchanger is inside the system. For

the desorption process, the hydrogen is released from the top surface with the heating fluid to supply the required heat instead. Considering the passive thermal management method, the passive heat exchanger design optimisations include inner/outer fins and phase change materials (PCMs) [74].

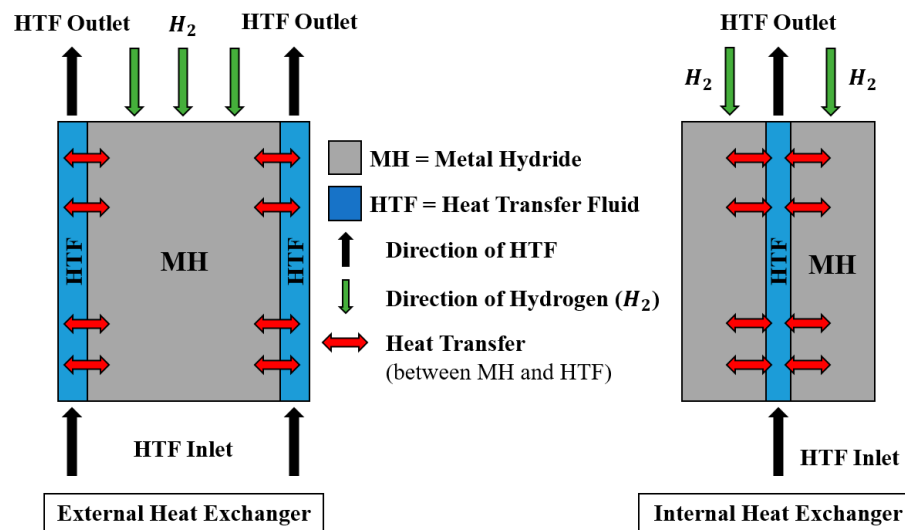


Figure 6. Schematic diagram of metal hydride storage system with external and internal heat exchangers for active thermal management method.

The schematic diagram of an MHHS with these heat exchangers under this method is provided in Figure 7. In this figure, it can be seen that the PCM is used to cover the MH bed as the external heat exchanger. There is heat transfer between these two parts. The PCM directly absorbs heat from the MH bed during hydrogen absorption and releases heat during hydrogen desorption. To improve heat transfer rate, the metal fins are integrated with the PCM and the MH bed. The heat is then transferred from the MH bed to the metal fin as well as from the metal fin to the PCM. The comparison of heat exchangers' performance in regard to the hydrogen sorption and heat transfer as well as reduction in volumetric and gravimetric parameters of the overall MHHS is provided in Section 3.4.

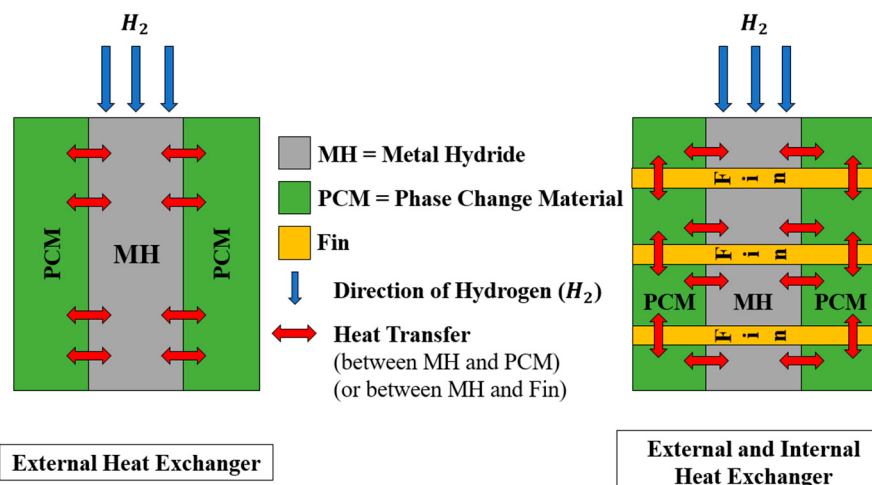


Figure 7. Schematic diagram of metal hydride storage system with external and internal heat exchangers for passive thermal management method.

3.1. Design Optimisation for Active Thermal Management Method

The active thermal management method requires external power to control the heat transfer rate. This method uses the HTF, such as air or water, to remove the heat during

the hydrogen absorption and provide the heat during the hydrogen desorption. The main advantages of the active method are ability to control the temperature of the storage system and faster heat removal/addition than offered by the passive method. There are two main types of heat exchanger configurations for the active method, which are external and internal heat exchangers.

3.1.1. External Heat Exchanger

The cooling/heating fluid is used as an external heat exchanger to cover the outer wall of the MH bed. Figure 8 presents an example of this heat exchanger design.

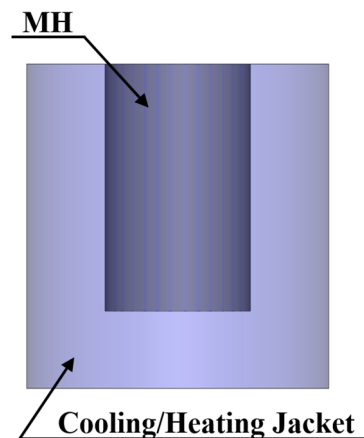


Figure 8. Example of an external heat exchanger design.

- Cooling/heat jacket

The reactor with the cooling jacket is widely used because of its simple structure and better heat transfer performance [75–82]. In the study of Chung and Ho [75], the expansion volume was used instead of porous media and located on the top of the MH bed, which was covered by water as a heating/cooling fluid. This study found that thermal resistance was increased by having an expansion volume inside the storage system. The two-dimensional MHHS with a cooling jacket was proposed by Patil and Gopal [80]. They found that supply pressure and initial HTF temperature affected hydrogen sorption rates. For fuel cell application, the poor thermal conductivity of the MH powder is the main problem for the high electrical power ratings of this application [82]. Although this technique is widely used due to the simple structure, the heat transfer areas are only near the outer wall of the MH bed which is connected to the cooling jacket. Therefore, this technique is usually combined with other internal heat exchanger techniques to increase heat transfer performance. The comparison between these heat exchangers and their performance is provided in Sections 3.3 and 3.4.

- Tube coil

An external tube coil was developed for a hydrogen storage canister with hot water as the HTF [83]. The hydrogen discharge rate was improved due to the hot water that was circulated around the LaNi₅ MH tank. Weiss-Ungethum et al. [84] performed an experimental study to investigate the effect of liquid cooling on the fuel cell stack by considering the various origins of heat loss. The three inner tubes were used to contain the NaAlH₄ material as MH powders covering the external helical coil tube. Their study indicated that the amount of heat loss that was rejected from the stack throughout the cooling fluid slightly exceeded the heat demand for the hydrogen discharging process. Therefore, comprehensive studies are required to design and optimise this heat exchanger for further improvement.

Although using an external heat exchanger also significantly increases heat transfer rate, this only applies to the outer wall of the MH bed which directly contacts the external heat exchanger wall. Therefore, various internal heat exchangers have been developed for better heat transfer distribution inside the MH bed's purpose.

3.1.2. Internal Heat Exchanger

Heat transfer surface area is generally increased by inserting the heat exchanger inside the MHHS, which increases the heat and mass transfer mechanisms [85]. Several studies have optimised heat exchanger performance by considering the development of multiple internal heat exchanger configurations to transfer cooling/heating fluid inside the MHHS. These include straight tubes, U-shape tube, mini-channel tubes, helical coil/spiral tubes, and semi-cylindrical coils. Figure 9 presents examples of different internal heat exchangers.

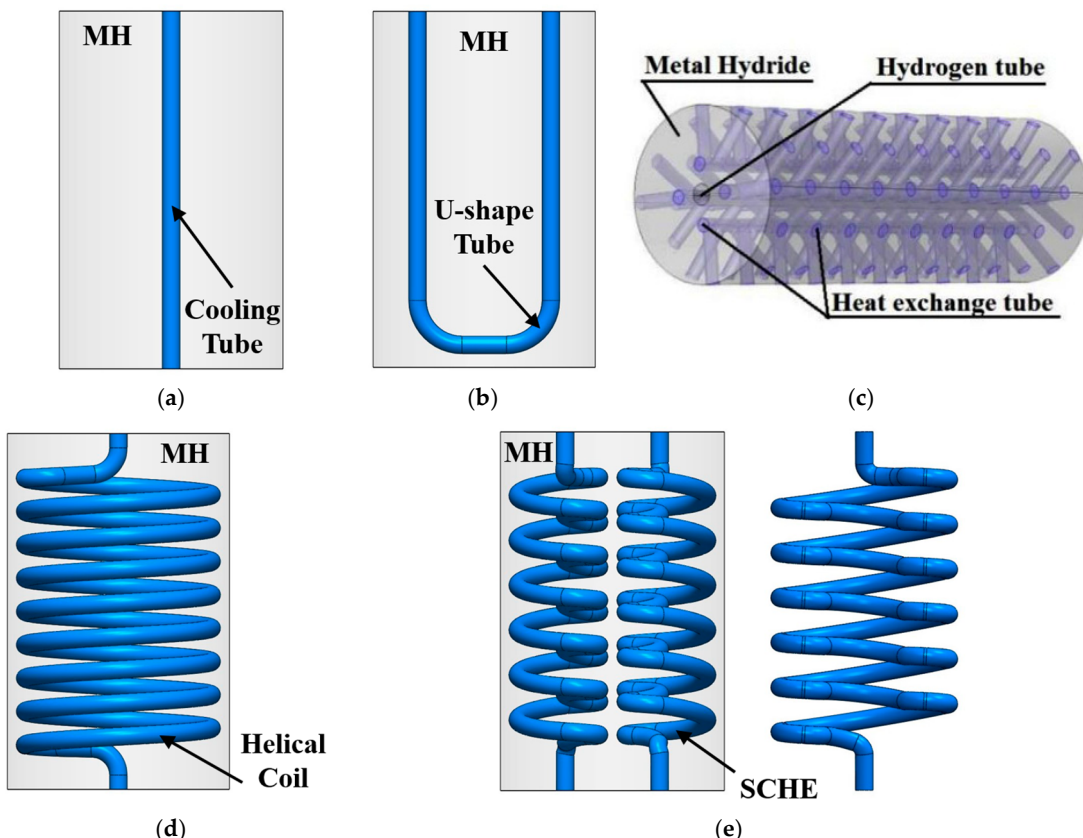


Figure 9. Examples of various internal heat exchanger designs: (a) Straight tube, (b) U-shaped tube, (c) Mini-channel tubes [86], (d) Helical coil, and (e) Semi-cylindrical coil.

- Cooling tube

The reactor was equipped with an internal straight tube heat exchanger for the HTF [87–95], as presented in Figure 9a. The HTF acts as a cooling/heating fluid to transfer generated heat or supply the required heat inside the MH bed during hydrogen absorption or desorption. The straight tube was embedded inside the LaNi₅ MH storage based on the combination of aluminium foam and hydride [89]. This study proved that using a metal foam exchanger and a concentric heat exchanger tube improved heat transfer performance, resulting in 60% improvement in absorption duration. Absorption duration decreased when using several straight tubes as the internal heat exchanger [90]. Multiple heat exchanger tubes were used for the heat transfer investigation during the hydrogen sorption by employing a hierarchical methodology [91]. The combination of two materials (LaNi_{4.3}Al_{0.4}Mn_{0.3} and Li-Mg-N-H) was used and filled inside the reactor by Bhouri et al. [92]. The design

optimisation for the number and thickness of tubes was evaluated under the absorption process. However, the study by Mohan et al. [93] proved that the thickness of several heat exchanger tubes had a minor effect on absorption and desorption time. Using several HTF tubes greatly influenced the MHHS rather than the HTF flow rate [94,95]. However, more uniform heat transfer distributions are still required for this technique. Therefore, other complex HTF structures have been performed to fulfil this requirement.

- U-shaped tube

Some researchers developed a U-shaped tube to increase the heat transfer area when it was inserted inside the tank. An example of this design can be seen in Figure 9b. A U-shaped tube incorporated with radial circular copper fins was placed inside LaNi₅ MH storage [96–98]. Water was used as the HTF and also to reduce the MH bed temperature during the absorption process. This study proved that the improvement in hydrogen charging time significantly depended on the number of fins, the thickness of fins, and the diameter of the heat exchanger tube. For the hydrogen absorption of 12 g, the absorption was reduced by 48% when the number of fins increased from 4 to 13. Increasing the diameter of the heat exchanger tube from 3.4 mm to 5.4 mm reduced absorption time by 27.6%. Increasing the fin thickness from 0.5 mm to 1.5 mm also improved absorption duration. However, these studies found that increasing the number of fins from 13 to 34 and reducing the fin thickness and pitch instead resulted in a 32% reduction in absorption time compared to the case with 13 fins. The ratio of the numbers of fins, pitch, and thickness was calculated under the constant volume of fins. The MHHS with a U-shaped tube should be incorporated with 34 radial circular fins with a pitch of 3.83 mm and a thickness of 0.19 mm. Therefore, under the constant volume of fins, the number of fins is the key parameter to improve heat transfer performance inside the MHHS. Recently, Yang et al. [99] performed a numerical study to further improve heat transfer and reaction rate performances. They combined the U-shaped tube with radial circular fins and additional bottom-curved fins. The results from these combinations proved that heat transfer performance significantly improved especially around the bend section of the U-shaped tube due to additional bottom-curved fins. The absorption rate significantly improved by 50% compared to the case without additional bottom-curved fins.

- Mini-channel tubes

The mini-channel tubes were designed as shown in Figure 9c. This technique contains multiple straight tubes (with a small diameter of 2–4 mm) inside the reactor for the HTF. The MH reactor, with the addition of mini-channel tubes based on the spiral tube design, was designed by Li et al. [100]. This study found that increasing the radius of the spiral tube resulted in faster reaction rate due to an increase in heat transfer surface area. Meng et al. [101] performed both numerical and experimental studies on the LaNi₅-based storage system based on multi-straight tubes. The comparison between various parameters, such as the number of straight tubes and hydrogen supply and discharge pressures, was performed. The results from this study indicated that the new reactor configuration improved the reaction rate for absorption and desorption processes compared to the traditional MHHS. The slim radiation tubes were designed for the HTF [86,102]. All radial heat exchange tubes were designed to connect to the cooling jacket around the MH bed. The MHHS with a radiation tube was compared to other reactors with different configurations such as straight and spiral tubes. The numerical results from the study indicated that using a radiation tube as a heat exchanger provided the best MHHS performance compared to other configurations. This was because of an increase in heat transfer surface area, resulting in more uniform temperature distributions inside the MHHS.

- Spiral/helical coil tube

Figure 9d provides an example of the spiral/helical coil tube. From this design, the secondary circulations of the coil tube significantly increase the heat transfer rate inside the MHHS as it offers more heat transfer surface area between the MH and the HTF compared to straight tubes [13,103]. Furthermore, it also generates the turbulence flow of the HTF during circulation along the HTF tube [104]. The more uniform temperature distribution inside the MHHS is the key factor for heat transfer enhancement by this technique [103]. A higher heat transfer coefficient was found in this method; in addition, it was easier to manufacture [105]. Under the constant HTF tube volume, hydrogen absorption duration was improved by 34.6% when using the spiral coil tube compared to the case with a straight tube [86]. Improving the absorption reaction by increasing the heat transfer coefficient was confirmed by Wang et al. [106]. Mellouli et al. [107] studied the effect of a spiral tube heat exchanger on the hydrogen absorption time when embedded in the MHHS. The inlet and outlet of this tube were designed to have the same direction to increase the tube length. Around the coolant tube, there was a faster hydrating reaction rate [108]. Reduction in coolant temperature resulted in faster hydrogen filling times [109,110]. A helical coil tube was used to circulate the supercritical water to heat the MHHS during the desorption instead of the electrical system [111]. The HTF's thermal diffusion technique was studied and applied by using the superheated water for the MHHS with a helical coil tube [112]. This study proved that thermal conductivity in MH has a lesser effect on the performance of the MHHS. The helical coil's characteristics also play a significant role in the enhancement of the heat transfer mechanism in the MHHS [113]. These include a smaller ratio of helical pitch to the helical diameter and non-dimensional pitch [13], increasing the number of flat spiral tube planes [114], a lower pitch of the helical coil, and a higher coil diameter [115]. Moreover, using the duplex helical elliptical tube [116] and a helical coil with a central return tube [115] greatly increased the heat removal rate between the HTF and the MH bed. However, it should be noted that the helical coil characteristics and their ratio are based on the MHHS scale.

- Semi-cylindrical coil tube

A semi-cylindrical coil tube from Figure 9e was developed from the helical coil tube to enhance heat transfer rate [117]. Two semi-cylindrical coil tubes were embedded inside the MHHS as internal heat exchangers. Due to the better heat transfer surface area arrangement of these heat exchangers, which resulted in having more uniform temperature distribution, the average bed temperature of the MHHS reduced faster than in the case with a conventional helical coil tube. Under constant volume of the MH bed and the HTF tube, the absorption duration significantly reduced by 59% compared to the storage with a helical coil case. Moreover, the semi-cylindrical coil tube also obtained a higher turbulence level of the HTF than the helical coil tube, resulting in faster heat removal [118]. Moreover, when combining the semi-cylindrical coil tube with the central return tube, heat transfer performance was greatly improved, resulting in faster hydrogen absorption/desorption [119,120]. The duration of the absorption/desorption cycle was reduced by 50% when using this heat exchanger compared to the case with the helical coil. There was a 31% reduction in the duration of the absorption/desorption cycle when using this heat exchanger with a central return tube compared to the case without this central return tube.

According to the above-mentioned information, to improve the overall MHHS performance, there are several internal heat exchanger configurations that have been designed instead of the conventional straight tube. Most recent studies have been focused on the internal heat exchanger rather than the external heat exchanger. This might be because the internal heat exchanger offers a higher heat transfer surface area. The enhancement

of heat transfer performance by the internal heat exchanger usually depends on the well arrangement of the heat exchanger structure, which increases heat transfer surface area and achieves more uniform temperature distribution. Furthermore, the complex heat exchanger structure also results in a higher turbulent flow, which significantly leads to faster heat transfer. However, all of these heat exchangers are obtained using the active thermal management method, which requires additional energy to transfer the heat. The other heat exchanger designs under the passive technique are provided in the next section. It is worth mentioning that the comparison between various internal heat exchangers and their performance can be found in Section 3.4.

3.2. Design Optimisation for Passive Thermal Management Method

Passive thermal management is a method that does not require any additional energy to improve heat transfer rate. This method normally uses natural convection, which can be achieved by adding fins or phase change materials to the inner or outer surface of the MHs. This technique usually requires materials with high conductivity which leads to an increase in heat transfer surface area. The main advantages of the passive method are easier implementation and lower cost to produce compared to the active method. This section provides a summary of the three main types that are usually applied to this method. These include the metal fins, metal foam, and phase change materials (PCMs).

3.2.1. Fins

Using fins as the external or internal heat exchangers is also one of the effective techniques to enhance heat transfer performance. The examples of fin heat exchanger designs are provided in Figure 10.

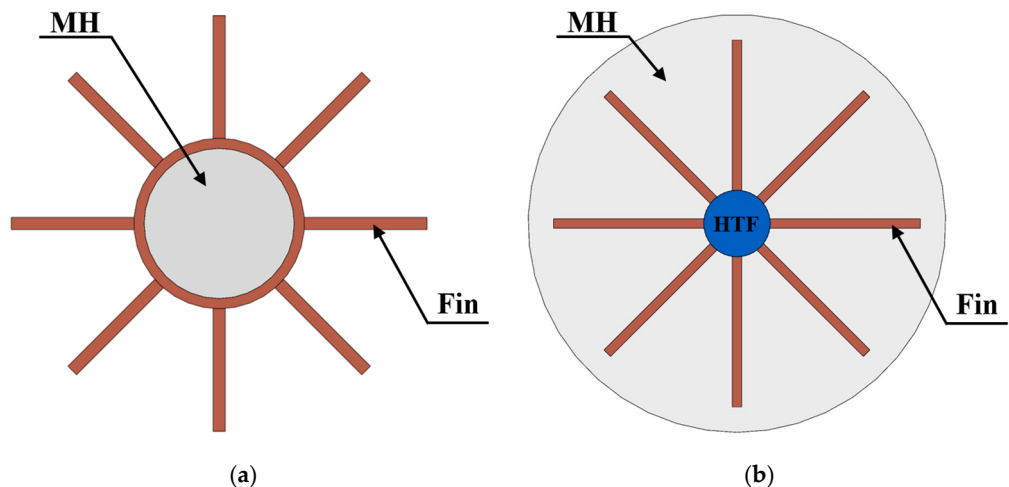


Figure 10. Examples of heat exchanger design and optimisation by using fins: (a) External fins and (b) Internal fins.

- External fins

Adding metal fins on the outer wall of the MH bed as an external heat exchanger is one of the external heat exchanger configurations which can increase the convective heat transfer area. An example of this design is provided in Figure 10a. An experimental study from Andreasen et al. [121] found that using axial fins as the external heat exchanger of the MH tank incorporated with internal disk-shaped metal foils significantly improved heat exchange with the environment. The MH reactor's performance mainly depended on the fin and tube arrangements [122]. Adding fins significantly affects the pressure of the hydrogen and the overall heat transfer inside the reactor [123]. The three full cycles

of hydrogen sorption (both absorption and desorption) were achieved in 15 min in the case with fins, while there was only one hydrogen desorption in the case without fins [123]. This means that there was an 83% improvement in hydrogen sorption when using fins compared to the case without fins. Although the sorption times can be further enhanced by increasing the fin area, this can increase the overall volumetric and gravimetric of the MHHS. Although external fins can provide a larger heat transfer area, there is only an increase in heat transfer area outside the MHHS reactor. Therefore, inserting fins inside the reactor as an internal heat exchanger is another way to improve the MH performance by maintaining natural convection conditions [124–128].

- Internal fins

Figure 10b provides an example of this design. The internal fin arrangement leads to a more uniform temperature distribution inside the storage system. Therefore, the local thermal conductivity of the MH bed can be improved because of an increase in the heat transfer area [128]. Keshari and Maiya [124] designed a new heat exchanger by using a copper pin fin for LaNi₅-based storage. Each pin fin was designed to attach them at the centre using side-by-side techniques. They concluded that the number of fins and fin diameter are the key parameters for pin fin heat exchanger design. Increasing the pin fin diameter and the number of fins further increased heat transfer surface areas, resulting in higher heat transfer rate. Krishna et al. [129] introduced the fin efficiency technique to optimise the conventional longitudinal fin performance. This study used the fin performance index to investigate the fin effect on hydrogen absorption/desorption. From their study under the total fin weight constant, the configuration with eight fins obtained the best performance compared to other fin numbers from four to twelve. The fin performance index significantly increased from 0.58 to 0.96 when increasing the fin numbers from four to eight. However, the fin performance index only increased from 0.96 to 1.1 when increasing the fin numbers from eight to twelve.

From this technique, increasing the fin number is the key parameter to improve heat transfer rate. However, the drawback of this technique also relates to the weight of overall MHHS, especially for mobile applications. Furthermore, this technique is usually combined with an internal cooling tube as it provides better heat transfer performance instead of having a natural convective heat transfer by using fins only. The well arrangement of the heat exchanger designs based on the fins and internal cooling tubes might be another option to reduce the weight of the overall storage system. These combinations are discussed in Section 3.3.

3.2.2. Metal Foam

Metal alloys (before forming the MH) usually have low thermal conductivity, negatively affecting the hydrogen reaction kinetics. Therefore, adding the metal foam improves the effective thermal properties of the MH bed. In general, the selected metal foam should have high thermal conductivity, and its porosity should be over 90% [73]. The comparison of the use of metal foam for the MH storage system was proposed under the different metal materials, including aluminium, copper, and zinc [89]. Numerical calculation was performed for the LaNi₅-based storage under the operating conditions at 293 K of the temperature and 0.1 MPa of supply pressure with the cooling fluid for convective heat transfer. This study proved that adding metal foam significantly improved the hydrogen absorption reaction. Absorption duration was improved by 55% in the case when zinc foam was added, 63% in the case when copper foam was added, and 66% in the case when aluminium foam was added compared to the case without metal foam. Figure 11 summarises the hydrogen absorption duration at 13 g of hydrogen/kg of hydride corresponding to the use of metal foams.

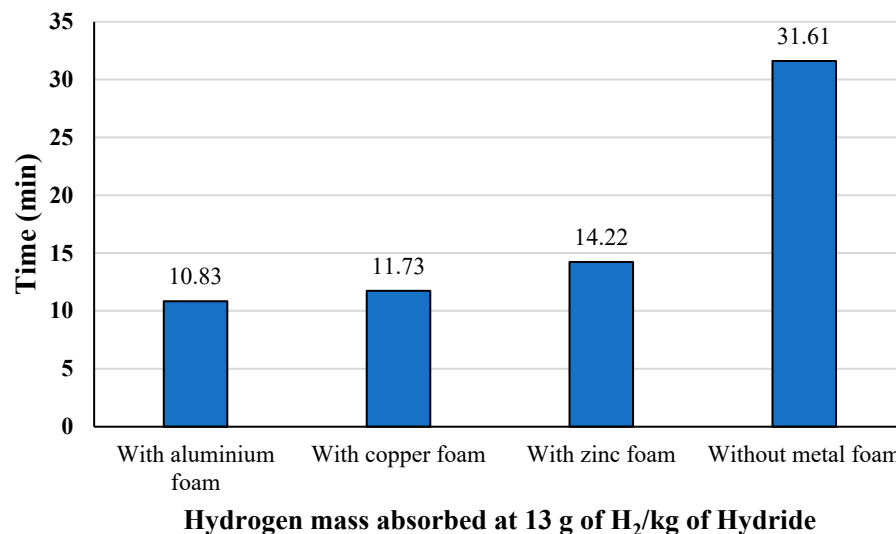


Figure 11. The hydrogen absorption duration from the use of metal foams to increase effective thermal conductivity; the study of Mellouli et al. [89].

Other studies also focused on adding aluminium foam for ETC improvement as this material offered higher thermal conductivity and lower thermal mass than other metal foams [130–134]. The overall ETC based on the aluminium foam addition was improved by 4 W/mK for MmNi_{4.5}Al_{0.5} storage [135] and up to 10 W/mK for LaNi₅ storage [136]. The porosity size also affected hydrogen reaction kinetics as the overall ETC significantly increased from 4.95 W/mK to 24.15 W/mK when reducing porosity from 98% to 90% [137]. However, the MHHS with metal foam is usually combined with a simple heat exchanger such as internal straight tubes [88], phase change material jacket [138], inner tubes, and cooling jacket [89,133]. This is because of the metal foam's structure and porosity. Moreover, enhancing the ETC by adding metal foam directly increases the weight of the overall storage system and reduces hydrogen storage capacity, which directly affects the overall MHHS performance in all MHHS scales. Disintegration during the hydrogen absorption/desorption is also the main problem of this technique [15]. Therefore, the most recent studies mainly focus on the improvement in heat transfer performance by the management of heat exchanger configurations rather than adding metal foam. One of the passive thermal methods that has been recently used for the MHHS is the use of PCM.

3.2.3. Phase Change Materials

Phase change materials (PCMs) have been used to improve the cooling and heating of the MHHS during the absorption and desorption processes due to their ability to provide high thermal energy storage capacity, chemical stability, and low costs [15]. Therefore, various PCMs have been applied in MHHS and several thermal management applications, such as the cooling of electronic devices [139,140] and the thermal management of batteries and buildings [141–143]. One of the key advantages of using PCMs is their ability to recover the waste heat during hydrogen sorption as the PCM absorbs the generated heat during the hydrogen absorption and releases it as the required heat during hydrogen desorption [144]. In general, PCMs such as paraffin and sodium nitrate (NaNO₃) have low thermal conductivity, resulting in the limitation of heat transfer rates. Therefore, several PCMs with high thermal conductivity have been proposed to solve this problem, such as LiNO₃·3H₂O, Mg₆₉Zn₂₈Al₃, and Na₂CO₃·10H₂O. In general, these PCMs have their own melting point temperatures and other thermo-physical properties. For this purpose, the different melting temperatures play a significant role in selecting which PCM to use with a

specific metal alloy. Table 4 summarises the selection of PCMs and their thermo-physical properties that have been used to improve the overall MHHS performance.

Table 4. Summary of selected phase change materials and their thermo-physical properties for some commonly used metal alloys.

Metal Alloy	PCM					
Type	Type of Selected PCM	Melting Temperature (K)	Density (kg/m ³)	Specific Heat (J/kg K)	Thermal Conductivity (W/m K)	Latent Heat of Fusion (kJ/kg)
LaNi ₅	Rubitherm (Salt) SP29Eu [138,145]	302.15–304.15	2000	2500	0.6	175
LaNi ₅	Paraffin RT35 [146,147]	308.15	880	1800	0.2	157
LaNi ₅	Paraffin [148]	308.15	850	2160	0.25	220
LaNi ₅	Paraffin RT28 [149]	301	880	1800	0.2	245
LaNi ₅	LiNO ₃ ·3H ₂ O [149–153]	303.3–305.3	2140	1730	1.32	296
LaNi ₅	Na ₂ CO ₃ ·10H ₂ O [149]	305	1460	1880	1.25	267
LaNi ₅	Na ₂ SO ₄ ·10H ₂ O [149]	305.5	1485	1440	1.23	251
LaNi ₅	CaCl ₂ ·6H ₂ O [149]	302.6	1802	1430	1.09	192
Mg	Mg ₆₉ Zn ₂₈ Al ₃ [154,155]	607	2900	1100	10	175
Mg ₂ Ni	NaNO ₃ [114,120,130,131, 156–158]	579–580	2260	1820	0.48	174
Mg ₂ Ni	NaOH [132]	590–591	2100	2080	0.92	165
Mg ₂ Ni	Mg ₆₉ Zn ₂₈ Al ₃ [159]	607	2900	1100	10	175
MmNiMnCo	RT35HC [157]	308.15	880	2000	0.2	240

In Table 4, it can be seen that there are only four metal alloys that have been incorporated with PCMs. A LaNi₅ alloy is mostly used as an MH material, followed by Mg₂Ni alloy. The LaNi₅ alloy has a high thermal conductivity of up to 1.5 W/mK and requires a low operating temperature, around room temperature at 293 K, to activate the system. However, this alloy has a low hydrogen storage capacity of up to 1.4 wt%. Mg₂Ni offers high hydrogen storage capacity with up to 6 wt%, but a high operating temperature of around 573 K is required to activate the system. Furthermore, this alloy also has a low thermal conductivity with less than 1 W/mK. A higher operating temperature range of Mg-based material must be used with a high melting temperature PCM such as NaNO₃. The MH materials and their thermal physical properties are provided in Sections 2.2–2.4.

The design configurations using PCM also influence the overall MHHS performance. Several PCM configurations have been designed to optimise PCM performance. These

can be classified into four main types: pool bed PCM, jacket bed PCM, spherical bed, partition arrangement PCM, and sandwich bed PCM. Figure 12 provides an example of these configurations.

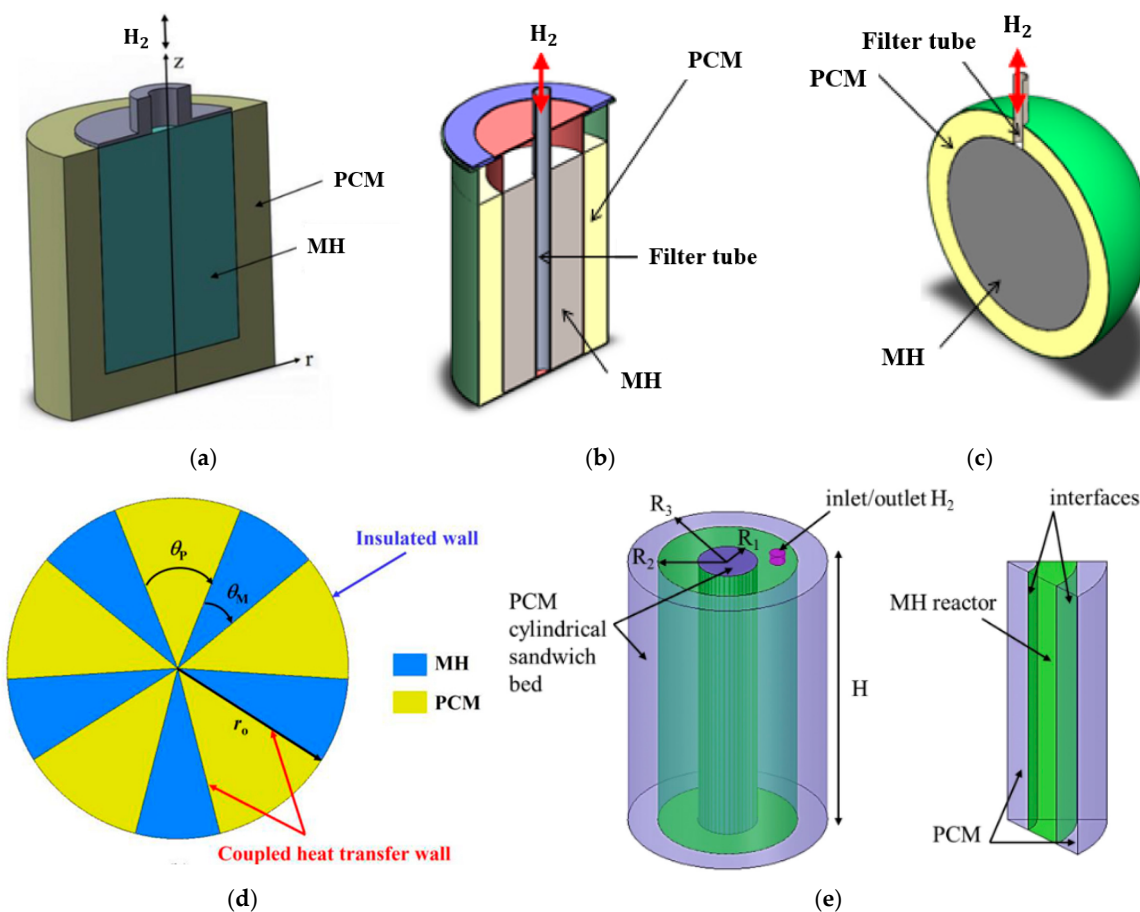


Figure 12. Design optimisation for various configurations of using phase change materials: (a) Pool bed [150], (b) Jacket bed [155], (c) Spherical bed [155], (d) Partition arrangement [160], and (e) Sandwich bed [131].

- Pool bed

The MHHS is designed by having a PCM covered around the MH bed except for the top side as the pool bed. The MHHS with a PCM pool bed can be seen in Figure 12a as an example. Maad et al. [152,153] used $\text{LiNO}_3 \cdot 3\text{H}_2\text{O}$ as the PCM to improve heat and mass transfer during the absorption of LaNi_5 MH storage. They found that the PCM's thermal conductivity and melting enthalpy were mostly affected by the hydrating rate and the capacity of MHHS. Then, this reactor was further used with Mg_2Ni as MH powder and $\text{Mg}_{69}\text{Zn}_{28}\text{Al}_3$ as the PCM [159]. This study summarised that a specific melting temperature, a high melting, and latent heat were essential for selecting PCM during hydrogen desorption. Due to the low thermal conductivity of the PCM, the metal foam was composited with PCM to improve heat transfer performance [138,146,149]. The results from these studies proved that inserting metal foam in the PCM improved thermal conductivity and reduced hydrogen sorption duration. Using copper foam with PCM obtained better MH storage performance compared to the PCM with aluminium foam [149]. Moreover, increasing PCM thermal conductivity positively improved the storage system [146]. Several PCMs were tested for the LaNi_5 MH storage by Mghari et al. [149]. These included Paraffin RT28, $\text{LiNO}_3 \cdot 3\text{H}_2\text{O}$, $\text{Na}_2\text{CO}_3 \cdot 10\text{H}_2\text{O}$, $\text{Na}_2\text{SO}_4 \cdot 10\text{H}_2\text{O}$, and $\text{CaCl}_2 \cdot 6\text{H}_2\text{O}$. It was summarised that the use of $\text{LiNO}_3 \cdot 3\text{H}_2\text{O}$ as PCM achieved better storage performance compared to

other PCMs, as the storage with $\text{LiNO}_3\text{-}3\text{H}_2\text{O}$ achieved a faster hydrogen absorption. The LaNi_5 -based MH storage with paraffin enhanced storage efficiency by 47% [147].

- **Jacket bed**

Unlike pool bed PCM, the jacket bed PCM only covers the MH bed like the outer cooling heat exchanger. Figure 12b presents an example of the MH reactor with a PCM jacket. Nguyen and Shabani [157] proposed MHHS for a solar system using PCM. They employed MmNiMnCo as the MH alloy and paraffin as a PCM. They stated that the thermal conductivity of PCM must be improved to 1.5 W/mK as a minimum value. With this minimum value, thermal management could be more practical. Lewis and Chippar [151] analysed the effect of the PCM on the MHHS during absorption and desorption processes. They used $\text{LiNO}_3\text{-}3\text{H}_2\text{O}$ as the jacket PCM and LaNi_5 as the MH alloy. In addition, they also investigated the effect of metal foam that was added to the PCM. This study proved that adding metal foam into PCM significantly improved storage performance.

- **Spherical bed**

A PCM configuration was designed to cover the MH bed as a spherical shape in the study by Melloui et al. [155], which is presented in Figure 12c. This configuration was compared to the base case with a PCM jacket bed. This study employed Mg as the MH powder and $\text{Mg}_{69}\text{Zn}_{28}\text{Al}_3$ as a PCM. This study showed that using the spherical tank to contain the PCM resulted in higher storage performance. Hydrogen sorption time improved by 22% with the use of a spherical tank compared to a jacket tank.

- **Partition arrangement**

Recently, a study by Dai et al. [160] proposed the new PCM configuration with the constant PCM and MH volumes by focusing on the effect of partition arrangement of the MH and PCM on hydrogen absorption performance. This can be seen in Figure 12d. The results from this study proved that when increasing the number of partitions from two to five, the hydrogen absorption duration was reduced by 23.8%. However, hydrogen absorption duration was significantly reduced by 67.13% when using the five PCM partitions instead of the PCM jacket.

- **Sandwich bed**

Increasing the PCM layer is also one of the effective techniques that can improve storage performance. The MH bed is placed in the middle between PCM beds, which can be seen in Figure 12e. A comparison between the MHHS with a PCM cylindrical jacket and the MHHS with a PCM cylindrical sandwich bed was performed by Alqahtani et al. [131]. The Mg_2Ni was employed as the MH material and NaNO_3 as the PCM bed. The results from this study proved that using a PCM sandwich bed resulted in a better heat transfer rate. Under the same PCM volumes, the durations of hydrogen absorption and desorption from the case with the sandwich bed were reduced by 81.5% and 73% compared to the case with the jacket bed. Ye et al. [161,162] used a PCM which was placed in the middle between two MH disks for heat recovery during the hydrogen desorption process. This study employed Mg as the MH powder and NaNO_3 as the PCM. When using PCM as a sandwich bed, desorption significantly improved by 21.8% compared to the case when PCM was used as a jacket bed. The design configuration of the PCM sandwich was then improved by using two different PCM materials with different melting points that were placed separately as two layers covering the area around the MH bed [132]. The NaOH PCM was placed next to the MH bed as the first layer, followed by NaNO_3 PCM as the second layer. This study proved that having two PCM layers with different PCM types improved hydrogen absorption duration by 26% and desorption duration by 51% compared to the PCM sandwich bed with the same PCM types. However, this design was suggested

for use with large-scale stationary storage (i.e., concentrated solar power applications) when considering the weight of the overall storage system and hydrogen storage capacity. Table 5 provides the summary of MH reactor configurations by using PCM.

Table 5. Summary of the configuration designs for using phase change materials with a metal hydride storage system.

Metal Alloy	PCM	Configuration of PCM	Reference
LaNi ₅	Rubitherm (Salt) SP29Eu	Pool bed	[138,145]
LaNi ₅	Paraffin RT35	Pool bed	[146,147]
LaNi ₅	Paraffin	Pool bed	[148]
LaNi ₅	Paraffin RT28	Pool bed	[149]
LaNi ₅	LiNO ₃ ·3H ₂ O	Pool bed	[149–153]
LaNi ₅	LiNO ₃ ·3H ₂ O	Jacket bed	[162]
LaNi ₅	LiNO ₃ ·3H ₂ O	Partition arrangement	[160]
LaNi ₅	Na ₂ CO ₃ ·10H ₂ O	Pool bed	[149]
LaNi ₅	Na ₂ SO ₄ ·10H ₂ O	Pool bed	[149]
LaNi ₅	CaCl ₂ ·6H ₂ O	Pool bed	[149]
Mg	Mg ₆₉ Zn ₂₈ Al ₃	Pool bed	[154]
Mg	Mg ₆₉ Zn ₂₈ Al ₃	Jacket bed, Spherical bed	[156]
MgH ₂	NaNO ₃	Sandwich bed	[103]
Mg ₂ Ni	NaNO ₃	Jacket bed	[114,157]
Mg ₂ Ni	NaNO ₃	Sandwich bed	[131,158]
Mg ₂ Ni	NaNO ₃	Capsule bed	[120]
Mg ₂ Ni	NaNO ₃ + NaOH	Cascaded sandwich bed	[132]
Mg ₂ Ni	Mg ₆₉ Zn ₂₈ Al ₃	Pool bed	[159]
MmNiMnCo	RT35HC	Jacket bed	[157]

Several types of PCM have been used for the MHHS with various metal alloys. The PCM sandwich bed achieves the best heat transfer performance of the MHHS as the generated heat from the MH bed transfers via two interfaces of the PCM. There is an over 22% improvement in hydrogen absorption/desorption based on the PCM sandwich bed compared to the case with the PCM jacket bed and pool bed. There is an over 26% improvement in hydrogen sorption when using two types of PCMs compared to only a single PCM under the PCM sandwich configuration design. Adding metal foam to the PCM is also another technique to increase PCM performance. However, using the PCM as a heat exchanger requires a large amount of PCM to absorb the removal heat during the hydrogen absorption and release the heat during the hydrogen desorption. The weight of PCM and metal foam has a drawback that affects the overall MHHS weight. Therefore, having the appropriate amount of PCM and metal foam is one of the key challenges for the overall MHHS design and optimisation.

As per the above-mentioned information, there are several types of heat exchangers for both external and internal types under the passive thermal management method. The overall weight of MHHS is the main problem of this method. This method generally requires a high amount of PCM to store the heat and release it when needed. Using a large number of fins also negatively affects the overall MHHS weight. Therefore, to further improve MHHS performance by considering the overall MHHS weight, the combination

of the heat exchangers between the active and passive thermal management methods has been recently proposed. The summary of this combination can be seen in Section 3.3.

3.3. Design Optimisation Based on the Combination of Various Heat Exchanger Methods

To further improve heat transfer performance as well as the overall MHHS performance, some studies have been focused on the combination of various heat exchanger types under active and passive thermal management methods. These include internal and external heat exchangers. Figure 13 provides examples of some heat exchanger combinations.

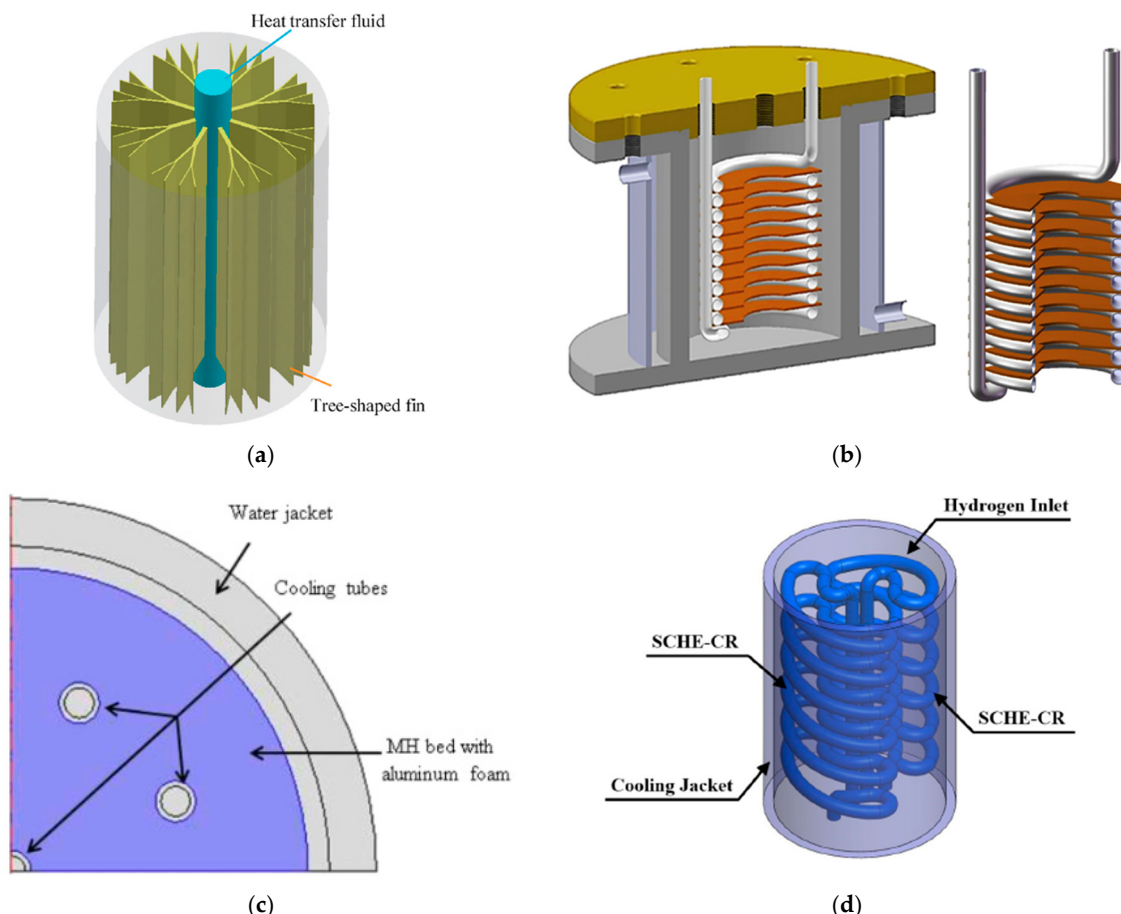


Figure 13. The example of the combination of various heat exchangers: (a) Central straight tube and fins [163], (b) Helical coil and fins [164], (c) Internal cooling tubes and cooling jacket [133], and (d) Semi-cylindrical coil with central return tube and cooling jacket [119].

- Active and passive thermal management methods

In Figure 13a,b, an internal straight tube or a helical coil tube is combined with internal fins to improve heat transfer performance and hydrogen reaction kinetics. Ma et al. [165] and Mallik and Sharma [166] developed the MHHS with multiple tubes combined with fins. This study found that the fin number was the key parameter that affected hydrogen absorption compared to fin radius and fins thickness. As shown in Figure 13a, tree-shaped fins were first introduced and embedded with a central heat exchanger tube by Bai et al. [163]. This design decreased the absorption time by 20.7% compared to the case with radial fins. Furthermore, increasing the length ratio of these fins increased the heat transfer performance of the MHHS. A variable cross-section annular fin was embedded with the MHHS's cooling tube to improve the inhomogeneous reaction phenomenon [167]. This study proved that using this fin effectively resolved the inhomogeneous reaction phenomenon in the hydrogen reaction process. Ayub et al. [168] performed a numerical

simulation of the MHHS with annular truncated hollow conical fins that were attached to the central cooling tube. They summarised that various fin parameters affecting the performance of the MHHS. These included fin angle, fin radius, number of fins, fin spacing, and fin thickness. The studies of Krishna et al. [129,169] proved that the appropriate selection of the fin number significantly affected heat transfer, while fin shape had a lesser effect on heat transfer performance. The fin thickness of 3 mm was recommended for the use of a precisely radial tapering fin. The helical coil tubes incorporated fins proposed by Dhaou et al. [170] and Souahila et al. [164]. This combination indicated that the absorption duration was two times lesser than in the case with a helical coil only. Figure 13b depicts the MH reactor with a helical coil tube and fins. Mellouli et al. [171] employed a spiral coil tube with additional circular fins that were embedded at the innermost turn. There was a 66% improvement in the absorption time in the case of those equipped with spiral coil tubes and circular fins compared to those without fins. Krishna et al. [172] proposed a new internal heat exchanger, namely a flat coil tube heat exchanger that was integrated with a spiral fin. From this combination, the hydrogen absorption duration reduced by 35.3% and 16.7%, compared to the case with a helical coil tube and double helical coil tube only.

- Active and active thermal management methods

The development of the MHHS with internal and external heat exchangers has been considered. Internal cooling tubes incorporating an external cooling jacket obtained better reaction kinetics [173,174]. The combination of internal straight tubes and an external cooling jacket was applied to a large-scale stationary application with Ti-Mn-based MHHS by Afzal and Sharma [133]. This combination design can be seen in Figure 13c. This study reported that a 14 MH multi-tube MH reactor had the best performance for the absorption and desorption processes, with the maximum reaction fraction at 1600 s, while the maximum reaction fraction from other cases was around 2700–3400 s. Larpruenrudee et al. [119] combined an internal semi-cylindrical coil heat exchanger and a central return tube with a cooling jacket (Figure 13d). This combination significantly improved heat transfer performance, resulting in faster hydrogen absorption reaction. Absorption duration was reduced by 51% when using these heat exchangers compared to the case without a cooling jacket.

Some studies also combined PCM with other heat exchanger types. The combination of PCM and inserting a heat exchanger into the MHHS also increases storage performance instead of adding metal foam into the PCM only. Figure 14 presents the examples of these combinations.

Mellouli et al. [156] studied the HTF tube's effect when embedded inside the MHHS that was covered by PCM. The new design of this MHHS configuration can be seen in Figure 14a. Multiple tubes were added to the MH bed to improve heat transfer rate. A numerical simulation was performed based on Mg₂Ni as MH material and NaNO₃ as the PCM. This study proved that the combination of these techniques (PCM jacket and internal cooling tube) improved the hydrogen absorption time by a 94% reduction compared to the base storage covered by PCM only.

In Figure 14b, it can be seen that this MHHS with outer PCM was combined with the inner copper fins to improve heat transfer performance [175]. The small MH parts were separated by the integration of inner copper fins in this study. This study concluded that using at least 10 copper fins reduced the hydrogen absorption rate by at least 86.5% compared to the case without fins.

Figure 14c shows the new MHHS configuration, which includes the outer PCM and the inner helical coil. Tong et al. [147] analysed the effect of using PCM with an internal cooling tube on the hydrogen desorption process. The helical coil tube was equipped with the MH bed (LaNi₅) covered by PCM (Paraffin RT35). Ardahaie et al. [114] employed the

NaNO_3 -based PCM jacket incorporating the internal spiral tube as the heat exchanger for the Mg_2Ni -based MHHS. This study summarised that employing a PCM jacket improved the hydrogen absorption and desorption time by 44% and 20%, respectively, compared to the base case without a PCM jacket. The $\text{LiNO}_3\text{-H}_2\text{O}$ -based PCM was employed for a LaNi_5 -based storage system with the concentric finned tube heat exchanger (a combination of straight tube and finned disc) [162]. This study proved that using jacket bed PCM reduced the absorption and desorption time by 50% compared to the case with a concentric finned tube heat exchanger only.

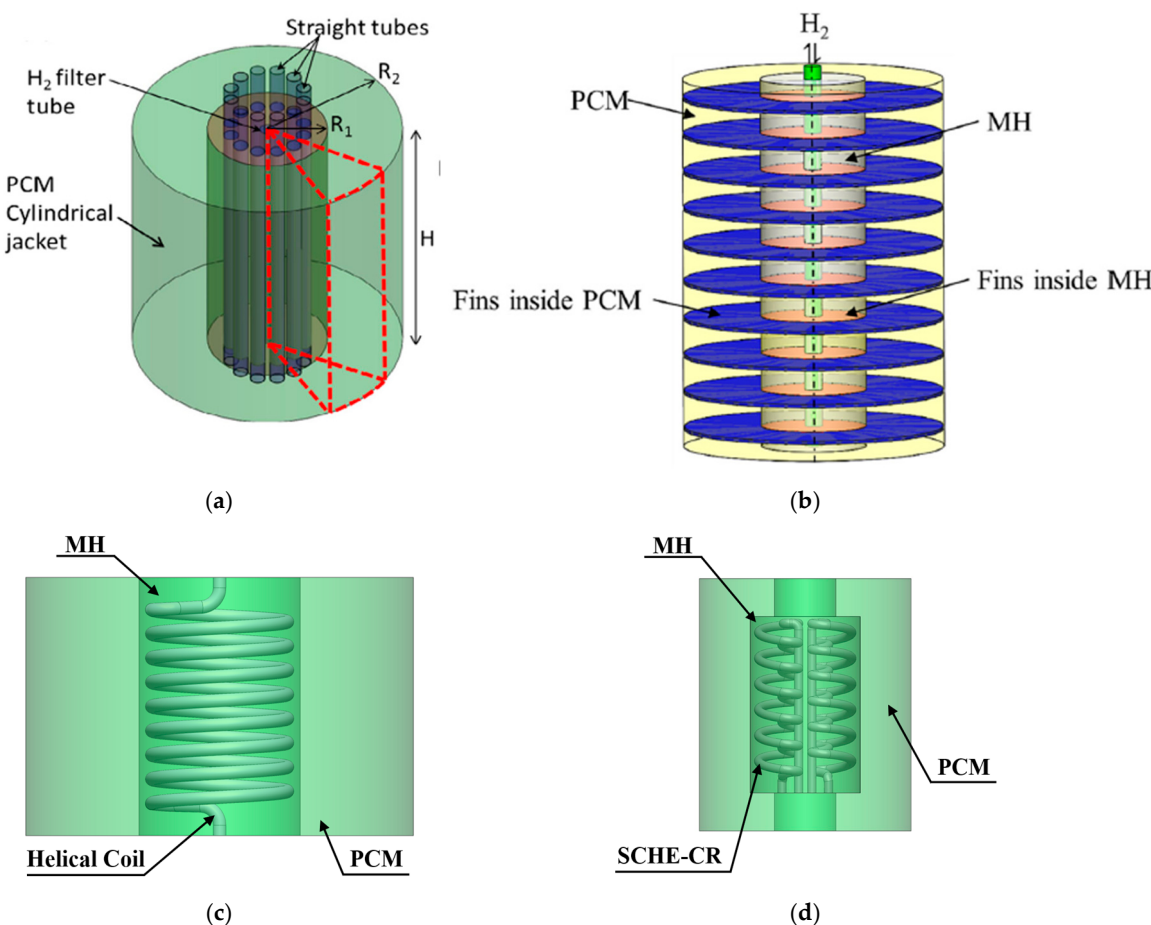


Figure 14. The combination of using phase change material and internal heat exchanger: (a) External PCM bed with internal cooling tube [156], (b) External PCM bed with fins [175], (c) External PCM bed with internal helical coil tube, and (d) External PCM capsule with internal semi-cylindrical coil tube.

Larprenrudee et al. [120] developed the new PCM configuration, namely the PCM capsule (see Figure 14d). The purpose of this development was to incorporate the internal heat exchanger, namely a semi-cylindrical coil heat exchanger with a central return tube. The results from this study proved that the duration of the hydrogen absorption/desorption cycle was reduced by at least 63% when using these heat exchangers compared to the case with PCM only. When using these heat exchangers, there was at least a 39% reduction in the duration of the absorption/desorption cycle compared to the case without PCM. This study also concluded that using the PCM capsule instead of the PCM jacket and the PCM pool bed resulted in better heat transfer performance. This is because of the well arrangement of the PCM capsule, which further increases heat transfer surface areas around the top and the bottom parts of the MH bed. Furthermore, this study also analysed the effect of PCM volume on the heat transfer/storage capacity and reaction of heat recovery rate. From the combination of these heat exchangers, 4/8 of the total PCM volume resulted in the best

performance with the heat transfer/storage capacity at 108.66 kJ of PCM and 146.71 kJ of the HTF and the heat recovery rate of the PCM at 42.55%. However, this study only analysed the effect of PCM volumes with additional heat exchangers on heat transfer/storage capacity. The effect of these volumes on the hydrogen absorption/desorption reaction rate has still not been considered.

From this section, it can be summarised that the overall heat transfer performance as well as the overall MHHS performance are significantly improved when combining several heat exchanger types. The combination of internal heat exchangers has its own drawback in that it can reduce the MH volume. Recently, the PCM has been used as the external heat exchanger. The required amount of PCM is mostly calculated based on assumption and its ability to store all the generated heat from the MH bed. In most studies, when combining the PCM with other internal heat exchangers, the relationships between the MH bed volume and the required amount of PCM (based on the heat exchanger combinations) are still not available yet. The proportional volume of PCM, MH bed, and HTF tube should be further considered to optimise MHHS performance. The effect of the proportional volume of these factors should be considered with the hydrogen absorption/desorption reaction rate.

To understand the effect of different heat exchanger designs on heat transfer performance, some studies performed the comparison between various heat exchanger designs. This can be seen in the next section.

3.4. Comparison Between Various Heat Exchanger Methods and Performance

An appropriate selection of heat exchanger type is one of the key factors to increase the overall MHHS performance. The enhancements of hydrogen reaction kinetics as well as the heat transfer mechanism are also achieved based on this factor. Several studies have been performed to compare MHHS performance under various heat exchanger types. The comparison between the effect of a cooling jacket and 22 circular fins on the MH performance was comprehensively investigated by Kaplan [176]. The results indicated that a higher hydrogen absorption rate was found when incorporated with a cooling jacket, as it significantly reduced MH bed temperature. The reactor with a cooling jacket achieved the highest effective thermal conductivity at $113 \text{ W/m}^2\text{K}$, while the case with external fins achieved only $35 \text{ W/m}^2\text{K}$. A study by Wu et al. [85] proved that the helical coil demonstrated the best performance to improve the heat and mass transfer rates compared to a straight tube and fins. The average reaction conversion for the desorption from the helical coil case reached 0.4 within 4000 s. The average reaction conversion for other cases was still less than 0.4 at 10,000 s. Another study by Tong et al. [177] also indicated that using a double-coiled tube resulted in a higher heat transfer rate than a straight tube and a single spiral tube. Askri et al. [178] performed a numerical simulation to compare the performance of various heat exchanger configurations. Their results indicated that employing both cooling tube and fins essentially reduced absorption time by 80%. However, using the internal cooling tube individually resulted in faster absorption time than using external fins only. Raju and Kumar [104] performed comparison between three heat exchanger configurations: (1) a cooling jacket with internal straight tubes and fins, (2) a cooling jacket with internal helical coil tubes, and (3) a cooling jacket with straight tubes that were placed horizontally. They proved that the MHHS with a cooling jacket and internal helical coil tube had better gravimetric and volumetric densities compared to other cases.

Various heat exchanger configurations for the MHHS were designed to compare performance and their effects on hydrogen storage capacity [179]. The designs included an inner straight tube, an inner helical coil, and a cooling jacket with and without fins,

which are presented in Figure 15a. Compared to other cases, storage with an inner straight tube resulted lower improvement in the dynamics of hydrogen absorption, followed by the case with a cooling jacket without additional fins. However, there was a similar absorption rate from storage with an inner helical coil and a cooling jacket with additional fins. Under the same operating conditions at 3 MPa of supply pressure and 303 K of storage temperature, the cases with helical coil and external cooling jacket with fins achieved an average hydrogen concentration of over 70% within 400 s, while the average hydrogen concentration from other cases was around 40–60% within 500 s. However, using an internal heat exchanger significantly reduced hydrogen storage capacity. The comparison of MH volume and reduction in storage capacity can be found in Figure 15b. The MH volume from the case with the internal helical coil was around 1 L, while the MH volume from other cases was around 1.2–1.4 L. Storage capacity was reduced by 23.7% when using an internal helical coil, while there was only an 8.1% reduction of storage capacity when using an internal straight tube and fins.

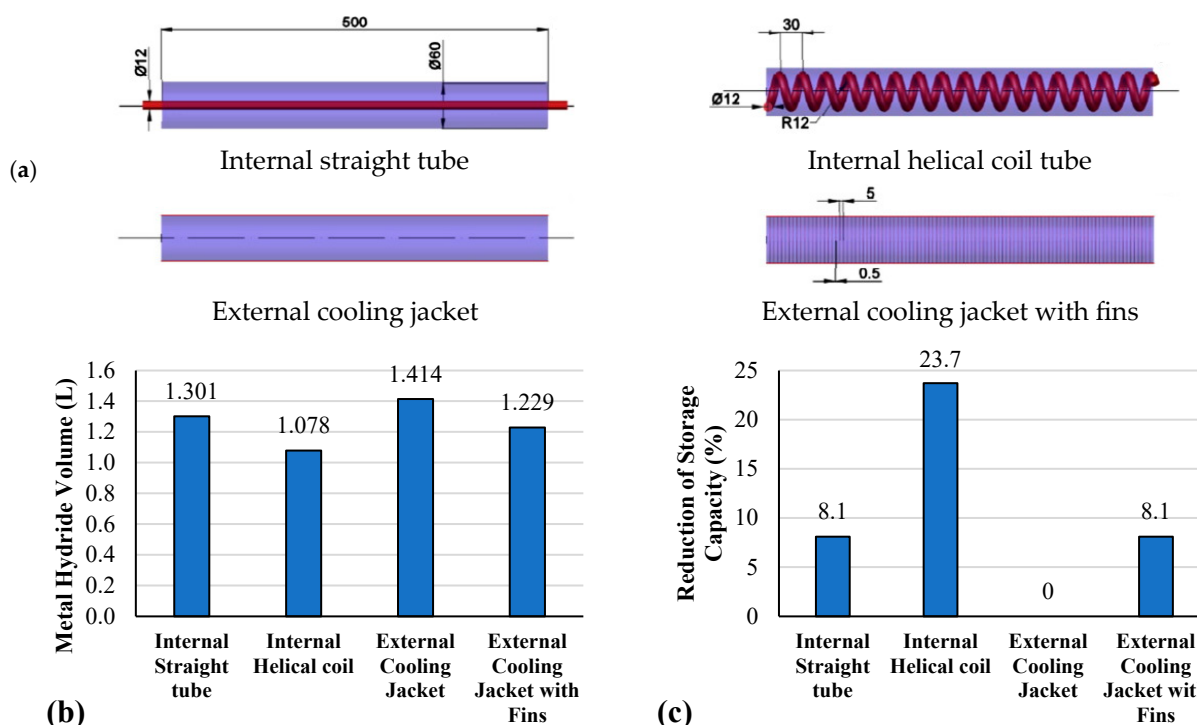


Figure 15. Effect of heat exchanger designs on the storage performance by Sekhar et al. [179]: (a) Four main heat exchanger designs, (b) Metal hydride volume, and (c) Reduction in hydrogen storage capacity.

Wang et al. [86] proposed the new LaNi₅-based MHHS design that was incorporated with radiation tubes (considered to be mini-channel tubes). They investigated the performance of mini-channel tubes by comparing this heat exchanger with other heat exchangers, including inner straight tube, convergent–divergent tube, spiral tube, conjugate spiral tube, coupling network spiral tube, and the case without a heat exchanger. These designs are provided in Figure 16. These heat exchangers were designed under the constant tube volume and an MH bed volume with operating conditions of 1 MPa of supply pressure and 293 K of initial temperature. At a 0.83 reaction fraction, the absorption duration from the case without a heat exchanger was at 2500 s, while it was only 1550 s in the cases with an inner straight tube and with the convergent–divergent tube. There was a 38% reduction in hydrogen absorption duration when using an inner straight tube compared to the case without a heat exchanger. However, the complete hydrating process was achieved

within 1200 s using a radiation tube. This resulted in 52% and 37% reductions in absorption duration when compared to the cases with a straight tube and a spiral tube, respectively. The absorption duration from the cases with other spiral tubes (conjugate and coupling network designs) was similar to the case with a normal spiral tube. Furthermore, absorption duration was significantly reduced by 77% when using a radiation tube compared to the case without a heat exchanger. This study concluded that the key reduction in hydrogen absorption from this study was the new arrangement of radial heat exchanger tubes, which improved the heat transfer mechanism in the radial section rather than the axial section of the MH bed.

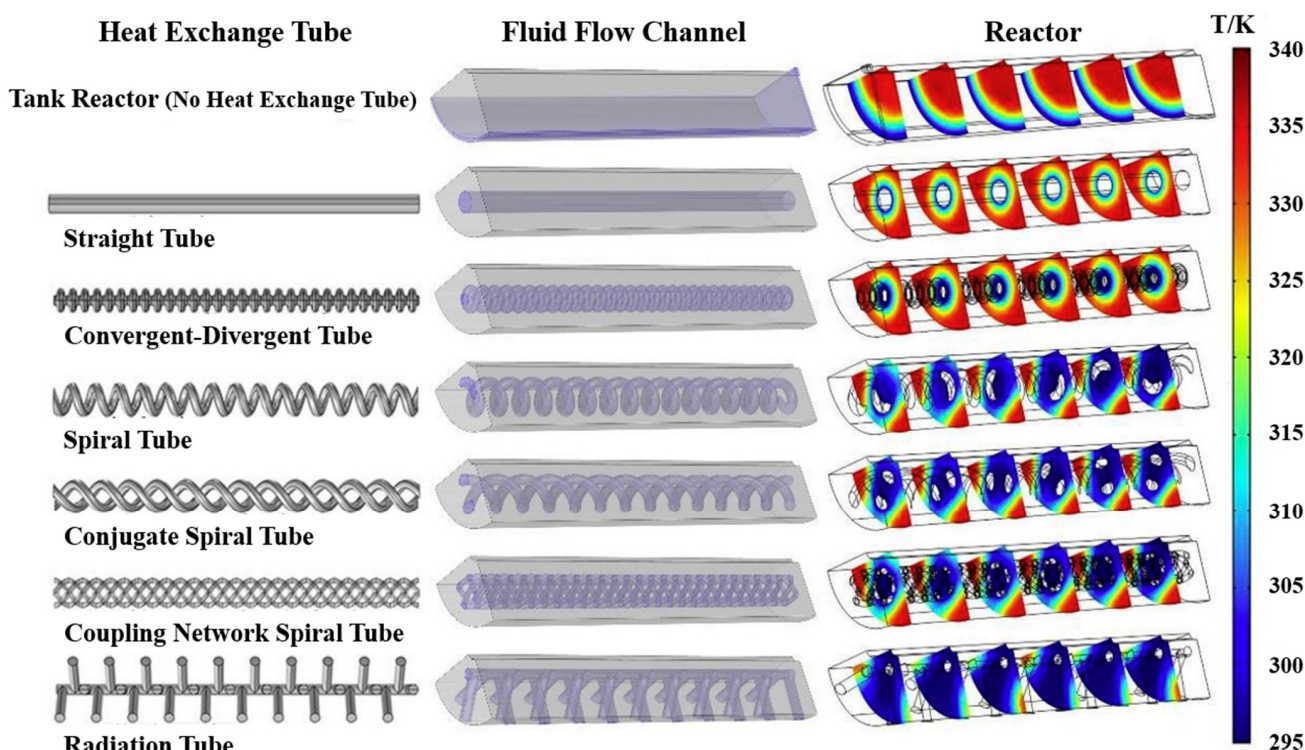


Figure 16. Comparisons of storage performance under various heat exchangers during the hydrogen absorption process of LaNi₅-based MHHS [86] (including the case without heat exchanger, straight tube, convergent–divergent tube, spiral tube, conjugate spiral tube, coupling network spiral tube, and radiation tube).

Zheng et al. [180] proposed the new MHHS design with primary and secondary helical tubes. The hydrogen tube was located at the central area of the MHHS to transport the hydrogen during absorption and desorption. The performance of this heat exchanger was analysed by comparing it with other heat exchanger designs, including the cooling jacket, mini-channel tubes, the spiral mini-channel tube, the duplex helical circular tube, and the duplex helical elliptical tube. Compared with the base case with the use of a cooling jacket, hydrogen absorption duration at 90% of concentration significantly reduced by 61%, 77%, and 83% when using a spiral mini-channel tube, a duplex helical circular tube, and a duplex helical elliptical tube instead of a cooling jacket, respectively. However, absorption duration was significantly reduced by 95% when using the primary and secondary helical tubes instead. This is due to the secondary spiral tube which accelerates both hydrating and heat transfer rate near the central area of the hydrogen tube.

In these comparisons, several heat exchangers and their performance have been compared to optimise MHHS performance with consideration of hydrogen reaction kinetics and heat transfer rate. These include internal and external heat exchangers such as inner/outer cooling tubes under different shapes (straight, helical coil, mini-channel tubes)

and fins. From these studies, it can be summarised that heat transfer rate and hydrogen reaction kinetics are based on the well arrangement/layout of the heat exchanger structure. This leads to a more uniform temperature distribution, resulting in greater reaction fraction distribution inside the MHHS. The active thermal management technique using the HTF throughout the heat exchanger tube (internal/external tube) significantly improves heat transfer efficiency in contrast to the passive thermal management technique such as fin and PCM. However, the drawback of the internal heat exchanger tube with complex structures based on the active thermal management technique is pressure losses. Huge pressure losses are usually a result of the curvature ratio of the complex HTF tube. This can negatively affect the overall MHHS performance. The amount of pressure losses from the heat exchanger should be stabilised to maintain the overall storage/heat exchanger performance [181,182]. Furthermore, the comparison between these heat exchangers and a U-shaped tube or a semi-cylindrical coil tube is still not available yet. Moreover, the combination of PCM configuration and these heat exchangers is also not available. As mentioned previously, the relationship between the required PCM volume, heat exchanger volume, and MH volume should be taken into account when combining the PCM with other internal heat exchangers as this can directly affect MHHS performance, especially for mobile applications. To optimise the MHHS, the effect of the proportional volume of these parameters should be considered with the hydrogen absorption/desorption reaction rate. The design optimisation of MHHS and heat exchangers usually depends on the MHHS application and its scale, which are based on the weight of the overall storage system and hydrogen storage capacity. However, it is not only heat exchanger design and configuration that affect the overall MHHS performance and heat transfer rates; heat transfer fluids (HTFs) also affect heat transfer performance. This is due to their thermo-physical properties that conduct heat. The next section provides a discussion based on the different HTFs on the heat transfer performance under hydrogen reaction kinetics.

3.5. Heat Transfer Fluids

Appropriate selection of HTFs affects heat transfer performance as well as hydrogen reaction kinetics. Several types of HTFs have been used for thermal energy storage. However, for MH storage, air and water are generally used as the HTF due to their low cost and lesser environmental impact. For the MH alloys which require operating room temperature at 298 K (i.e., LaNi₅), water is usually used as the HTF. However, the air is generally used with the MH alloys which require a higher operating temperature (i.e., Mg, Mg₂Ni) at 573 K. The effect of selecting HTF on hydrogen absorption performance was investigated by Mellouli et al. [156]. HTFs in this study included air, water, oil, and molten salt. Mg₂Ni was employed as the MH powder and NaNO₃ as the PCM. Investigation was performed under the operating temperature of the storage system and HTF of 579 K and a supply pressure of 1.5 MPa. Thermo-physical properties of these HTFs and the results of this investigation are summarised and provided in Table 6 and Figure 17.

Table 6. Thermo-physical properties of heat transfer fluids [183].

Type of HTF	Melting Point (K)	Viscosity (Pa s)	Thermal Conductivity (W/mK)	Heat Capacity (kJ/kgK)
Air	-	0.00003	0.06	1.12
Water/steam	273	0.00133	0.08	2.42
Thermal oil	253	0.014	0.136	2.25
Molten Salt	368	0.007	0.654	1.44

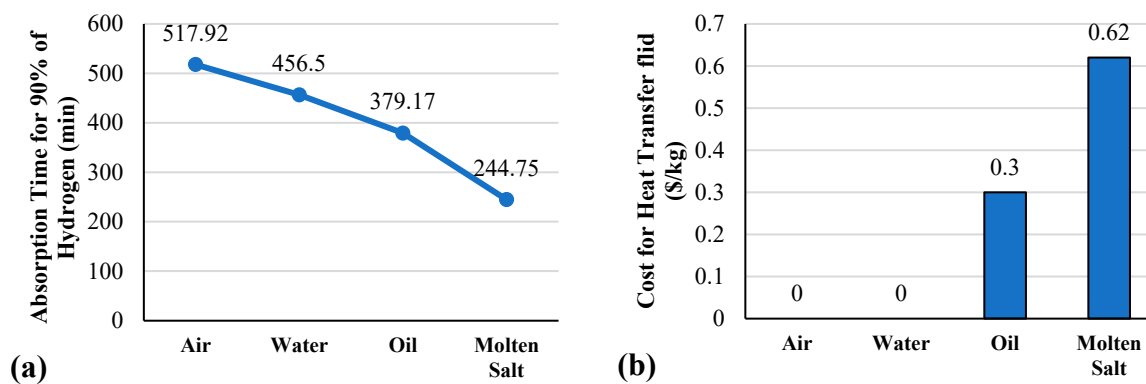


Figure 17. Comparison of the hydrogen absorption time and cost between various heat transfer fluids: (a) Absorption time for 90% of hydrogen and (b) Cost for heat transfer fluids per kilogram [156,183].

As per Figure 17a, air and water require longer hydrogen absorption time compared to oil and molten salt. The absorption time for the cases with air and water is over 400 min, while using molten salt requires absorption time of under than 300 min. In contrast, as per Figure 17b, using molten salt requires a large cost of approximately USD 0.62–0.81 per kilogram, while using oil also requires a high cost, around USD 0.3 per kilogram. However, air and water are preferred as there is no cost.

4. Operating Conditions

The operating parameters during the reaction process are the main factors that can positively or negatively influence hydrogen reaction kinetics as well as the overall MHHS performance in actual utilisation. The range of operating conditions can be varied due to the MH materials that have different thermo-physical properties. Therefore, the enhancement of the MHHS performance for both small- and large-scale operation has been considered based on the optimisation of operating parameters. The operating parameters basically include the initial temperature of MH storage, hydrogen loading pressure, initial temperature and flow rate of the HTF, heat transfer coefficient (HTC), effective thermal conductivity (ETC), and particle size.

4.1. Initial Condition of the Metal Hydride Storage

Appropriately selecting initial temperature and supply pressure plays a significant role in the hydrogen reaction kinetics during absorption and desorption. The initial temperature directly affects the driving force when producing the hydride reaction. For the hydrogen absorption process, decreasing the initial temperature results in faster absorption at the initial moment of the process. A lower initial temperature directly causes a lower equilibrium pressure. The hydrogen is then absorbed faster with a larger difference in pressure between exerted and equilibrium pressure. Therefore, a higher exerted pressure also leads to faster hydrogen absorption [13]. In general, the metal alloys significantly absorb the hydrogen at the initial moment of hydrogen absorption due to a larger difference between these two pressures [184,185]. However, the opposite is applied to the hydrogen desorption process. In the previous discussion under the introduction section, it was shown that due to the exothermic reaction for the hydrogen absorption process and the endothermic reaction for the hydrogen desorption process, a higher initial temperature usually results in faster desorption. The operating condition ranges for both temperature and pressure for some commonly used metal alloys can be seen in Table 2.

Various types of heat exchanger designs have been proposed recently. Among the heat exchanger designs using the HTF, some studies focus on improving MHHS performance based on the operating conditions of the system. As mentioned earlier, the operating

temperature and pressure ranges are dependent on MH materials, which have different operating ranges. The investigation of various initial temperatures of the storage was performed in a few studies based on the Mg₂Ni alloy due to the operating temperature ranges of MH materials. The initial temperatures at 573 K and 673 K were the best values for hydrogen absorption and desorption, respectively [85,117]. The loading pressure also varies depending on MH materials. Only three types of metal alloys have been used to compare the MH performance by focusing on loading pressure. These include LaNi₅, Mg₂Ni, and MmNi_{4.6}Al_{0.4}. The heat exchanger types are only the external cooling/heating jacket and the internal heat exchanger tube that require the HTF. The best case of LaNi₅-based storage incorporating a mini-channel heat exchanger was found when using supply pressures of 1 MPa and 0.1 MPa for hydrogen absorption and desorption, respectively. A supply pressure of 1.2–1.6 MPa is the best value for absorption and 0.025 MPa is the best for desorption with LaNi₅-based storage with an external cooling jacket [75,76,78]. The best value for Mg₂Ni-based storage during the absorption is 1.8 MPa for multi-zone configuration [186] and semi-cylindrical coil [117], while the best value for desorption is 0.8 MPa for the helical coil [85]. The best values of supply pressure during absorption and desorption for MmNi_{4.6}Al_{0.4}-based storage with an external heating/cooling jacket are 3 MPa and 1 MPa, respectively [80]. Table 7 summarises the initial condition of the MHHS based on the initial temperature and loading pressure that affect hydrogen absorption and desorption duration.

Table 7. Summary of initial conditions of metal hydride storage on the improvement in hydrogen sorption duration.

Initial Temperature of Metal Hydride Storage						
Metal Alloy	Heat Exchanger Types	Hydrogen Sorption	Temperature Range of Storage (K)	Improvement in Hydrogen Sorption (%)	Best Case (K)	Reference
LaNi _{4.7} Al _{0.3}	Straight tubes	Absorption	293–308	<1	293	[187]
Mg ₂ Ni	Helical coil	Absorption	523–673	NA	523	[13]
Mg ₂ Ni	Helical coil	Desorption	573–673	NA	673	[85]
Mg ₂ Ni	Helical coil with central return tube	Absorption	523–673	NA	523	[186]
Mg ₂ Ni	Semi-cylindrical coil	Absorption	473–623	11–24	573	[117]
Loading Pressure						
Metal Alloy	Heat Exchanger Types	Hydrogen Sorption	Pressure Range of Storage (MPa)	Improvement in Hydrogen Sorption (%)	Best Case (MPa)	Reference
LaNi ₅	Mini-channel	Absorption Desorption	0.5–2.5 0.0–0.2	42–62 21–63 (RF = 0.1)	1.0 0.1	[102]
LaNi ₅	Mini-channel	Absorption	0.7–1.6	43–65 (RF = 0.8)	1.0	[116]
LaNi ₅	Heating/cooling jacket	Absorption Desorption	0.4–1.6 0.025–0.1	58–63 (RF = 0.9) 37–50 (RF = 0)	1.6 0.025	[75]
LaNi ₅	Heating jacket	Desorption	0.025–0.1	31–66	0.025	[76]
LaNi ₅	-	Absorption	0.6–1.2	19–38	1.2	[78]
LaNi ₅	U-shaped tube and fin	Absorption	1.0–1.8	42.4	1.8	[99]

Table 7. Cont.

Metal Alloy	Heat Exchanger Types	Loading Pressure				
		Hydrogen Sorption	Pressure Range of Storage (MPa)	Improvement in Hydrogen Sorption (%)	Best Case (MPa)	Reference
LaNi ₅	PCM Partition arrangement	Absorption	0.8–1.6	41.23	1.6	[160]
LaNi _{4.7} Al _{0.3}	Straight tubes	Absorption	2.5–3.5	30 (Cap = 1.28 wt%)	2.5	[187]
			Lower values could not reach 1.28 wt%			
Mg ₂ Ni	Helical coil	Absorption	0.6–1.8	62–75 (RF = 0.7)	1.8	[115]
Mg ₂ Ni	Helical coil	Desorption	0.8–1.6	35–76 (RF = 0.1)	0.8	[85]
Mg ₂ Ni	Multi-zone configuration	Absorption	1.0–1.8	38–48	1.8	[186]
Mg ₂ Ni	Semi-cylindrical coil	Absorption	1.2–3.0	32–42	1.8	[117]
MmNi _{4.6} Al _{0.4}	Heating/cooling jacket	Absorption	1.0–3.0	45–72 (RF = 0.9)	3.0	[80]
		Desorption	1.0–3.0	20–53 (RF = 0.1)	1.0	

Note: RF = Reaction fraction (maximum reaction fraction that could be achieved for hydrogen absorption and minimum reaction fraction that could be achieved for hydrogen desorption by specific values) and Cap = Hydrogen storage capacity.

From these parameters, it is obvious that the different MH materials also have different initial temperatures and loading pressure ranges to activate the system. The lower initial temperature of MHHS usually results in better performance for the absorption process, while the higher initial temperature is better for the desorption process. In contrast, a higher loading pressure is usually better for absorption, while a lower loading pressure is suitable for desorption. However, it should be noted that appropriate range selection of these two parameters is required, especially when using the new MH materials as these parameters can significantly affect hydrogen storage capacity [16,117].

4.2. Initial Condition of the Heat Transfer Fluid

Several types of HTFs have been used for thermal energy storage. However, for the MHHS, air and water are generally used as the HTF due to their low cost and lesser environmental impact. A lower/higher HTF temperature directly improves heat transfer rate during the hydrogen absorption/desorption process. This results in faster hydrogen reaction kinetics in both absorption and desorption processes. A study by Ardahaie et al. [114] proved that reducing the HTF temperature from 573 K to 373 K improved absorption duration by 47%, while increasing the HTF temperature from 643 K to 843 K improved desorption duration by 43%. The turbulence level of the HTF flow rate also plays an important role in removing the generated heat during hydrogen absorption and supplying the required heat during hydrogen desorption [102]. A high turbulence level is caused by a high HTF flow rate that circulates through the HTF tube. A study of Anbarasu et al. [87,188–190] found that the operating pressure, the temperature of the cooling fluid, and the ETC of the MH impacted MH reactor performance. A faster hydrogen absorption/desorption reaction was observed when increasing the HTF flow rate [98]. However, a higher number of HTF tubes obtained a better MH performance compared to the HTF flow rate [94,95]. The initial HTF temperature should be lower than the initial MHHS temperature for the hydrogen absorption process. In contrast, the initial HTF temperature should be higher than the initial MHHS temperature for the hydrogen

desorption process. As for faster hydrogen reaction kinetics, the MHHS must be cooled down during the absorption, while the MHHS must be heated up during the desorption.

Table 8 summarises the initial conditions of the HTF and their effects on the improvement in hydrogen sorption duration under various heat exchanger types. A lower HTF temperature usually results in a higher hydrogen absorption reaction. In contrast, a higher initial temperature of the HTF leads to a higher hydrogen desorption reaction instead. The lowest initial temperatures for the hydrogen absorption at 283 K and 298 K are used for LaNi₅-based storage and MmNi_{4.6}Al_{0.4}-based storage, while the highest initial temperatures for the desorption process at 353 K and 400 K are used for these storages. The minimum initial temperature for the absorption at 373 K and the highest initial temperature for the desorption at 843 K are used for Mg₂Ni-based storage. However, some studies focus on improving the storage system by using various flow rates and Reynolds numbers (Re). In general, the flow rate and Re are varied depending on the heat exchanger tube's diameter. With a tube diameter of 6 mm of the semi-cylindrical coil, a Re value of 22,000 is the best value for Mg₂Ni-based storage [117]. When reducing this tube diameter from 6 mm to 4 mm, a Re value of 9000 is the best value for this storage type. With the tube diameter of 4 mm of the mini-channel, a flow rate of 1 m/s is the best value for LaNi₅-based storage [102].

Table 8. Summary of initial conditions of a heat transfer fluid on the improvement in hydrogen absorption and desorption duration.

Initial Temperature of Heat Transfer Fluid							
Metal Alloy	Heat Exchanger Types	Hydrogen Sorption	Temperature Range of HTF (K)	Improvement in Hydrogen Sorption (%)	Best Case (K)	Reference	
LaNi ₅	Mini-channel	Absorption	273–313	20–45	293	[102]	
		Desorption	333–373	25–56	353		
LaNi ₅	Mini-channel	Absorption	273–298	30–65 (RF = 0.8)	273	[116]	
LaNi ₅	Heating/cooling jacket	Absorption	283–323	38–72 (RF = 0.9)	283	[75]	
		Desorption	293–323	68–86 (RF = 0.4)	323		
LaNi ₅	Heating jacket	Desorption	293–323	34–61	323	[76]	
LaNi ₅	Spiral coil	Absorption	283–293	21–38	288	[107]	
		Desorption	303–323	60–69	323		
LaNi ₅	U-shape tube and fin	Absorption	273–313	55	273	[99]	
Mg ₂ Ni	Semi-cylindrical coil	Absorption	373–573	20–56	373	[117]	
Mg ₂ Ni	Semi-cylindrical coil with central return tube	Absorption	423–573	19–36	423	[119]	
		Absorption	423–573	15–26	423		
Mg ₂ Ni	Semi-cylindrical coil with central return tube and PCM capsule		573–723	25–38	723	[120]	
			643–843	31–47	373		
Mg ₂ Ni	Spiral coil and PCM	Absorption	373–573	32–43	843	[114]	
		Desorption	643–843	31–47	373		
Mg ₂ Ni	Multi-zone configuration	Absorption	373–573	50–66	373	[186]	
MmNi _{4.6} Al _{0.4}	Heating/cooling jacket	Absorption	298–318	13–36 (RF = 0.9)	298	[80]	
		Desorption	380–400	15–39 (RF = 0.1)	400		

Table 8. Cont.

Flow Rate of Heat Transfer Fluid						
Metal Alloy	Heat Exchanger Types	Hydrogen Sorption	Flow Rate Range of HTF (m/s)	Improvement in Hydrogen Sorption (%)	Best Case	Reference
LaNi ₅	Mini-channel	Absorption Desorption	0.1–2.0 (m/s) 0.1–2.0 (m/s)	44 19	1.0 (m/s) 1.0 (m/s)	[102]
LaNi ₅	U-shaped tube and fin	Absorption	1.0–3.0 (m/s)	8.2–15.7	2.0 (m/s)	[99]
LaNi _{4.7} Al _{0.3}	Straight tubes	Absorption	10–35 (lpm)	21–38	20 (lpm)	[187]
Reynolds Number of Heat Transfer Fluid						
Metal Alloy	Heat Exchanger Types	Hydrogen Sorption	Re Range of HTF	Improvement in Hydrogen Sorption (%)	Best Case	Reference
Mg ₂ Ni	Multi-zone configuration	Absorption	17,000–52,000	13–19	52,000	[186]
Mg ₂ Ni	Semi-cylindrical coil	Absorption	10,000–22,000	28–50	22,000	[117]
Mg ₂ Ni	Semi-cylindrical coil with central return tube	Absorption	6400–14,500	12–24	9000	[119]

Note: RF = Reaction fraction (maximum reaction fraction that could be achieved for hydrogen absorption and minimum reaction fraction that could be achieved for hydrogen desorption by specific values and certain time).

From these parameters, it can be seen that a lower initial temperature of the HTF achieves better performance for the absorption process, while a higher initial temperature of the HTF is better for the desorption process. It is worth mentioning that the HTF temperature ranges from these studies might not be applied in reality. Appropriate selection of the HTF temperature ranges should be based on each specific application. For the HTF flow rate and Re, a higher value of these two parameters always achieves higher heat transfer performance as the heat is always transferred faster based on faster fluid flow. However, an appropriate selection of this parameter usually depends on HTF tube diameter. Moreover, in reality, a high-speed flow rate of the HTF or a high coil pitch/curvature ratio of the coil tube usually increases the oscillation level. This significantly affects the heat and mass transfer rate [191–193]. In some cases, these changes can induce flow instabilities in equipment due to the fluctuation of flow and pressure drop [194]. Therefore, a real experiment is required to test the MHHS system when applying the heat exchanger with the HTF at a high flow rate.

4.3. Other Operating Conditions and Comparison of the Operating Parameters

Other operating parameters have been analysed recently. These include the heat transfer coefficient (HTC) between the MH bed and the HTF, effective thermal conductivity (ETC), and particle sizes. Valizadeh et al. [76] studied the effect of the HTC between the MH bed and HTF for the LaNi₅-based storage that was covered by a heating jacket during the desorption process. The HTC varied from 500 W/m²K to 2000 W/m²K. Authors pointed out that the suitable value was 500 W/m²K. Other higher HTC values had a lesser effect on the desorption process. This was due to the limitation of heat capacity inside the MH bed. A study by Wu et al. [85] and Eisapour et al. [115] also proved that among the HTCs between 10 W/m²K and 1000 W/m²K, the HTC at 500 W/m²K was the best value for the desorption process of the Mg₂Ni-based storage system with an internal helical coil heat exchanger. Similarly, a study by Larpruenrudee et al. [119] also reported that using

the HTC at 500 W/m²K with semi-cylindrical coil heat exchangers with a central return tube and a cooling jacket resulted in the best heat transfer performance compared to other lower and higher HTC values. Li et al. [100] studied the effects of operating parameters and spiral mini-channel tubes on heat transfer efficiency and hydrogen absorption rate of LaNi₅-based storage. The operating parameters included volume fraction, loading pressure, initial temperature, ETC, and HTC. The study indicated that the HTC only had a lesser effect on the hydrogenation process compared to other parameters. Among the HTC from 500 W/m²K to 8000 W/m²K, there was only a 2% improvement in hydrogen absorption duration. In the ETC ranges from 0.5 W/mK to 7.5 W/mK, the recommendation value was 2.5 W/mK, with the improvement in the absorption reaction at 48% from the ETC at 0.5 W/mK. improvement inAbsorption reaction only improved by 29% when the ETC increased from 2.5 W/mK to 7.5 W/mK.

The effect of operating conditions was considered by a numerical study of Raju et al. [187]. The multi-tube heat exchanger was used as an internal heat exchanger for MH (LaM_{4.7}Al_{0.3}) storage. This study concluded that operating parameters, especially supply pressure, significantly affected the absorption process. The flow rate of the HTF also influenced hydrogen absorption. Several studies [106,108,115,163,195] also proved that the HTF temperature and loading pressure significantly influenced hydrogen reaction kinetics for both absorption and desorption compared to other parameters, including volume of MH storage, overall HTC, and initial temperature of the MHHS. Furthermore, the reduction in coolant temperature reduced the hydrating time by approximately 57% compared to the base case [109,110]. The multiple zones of HTF were proposed to improve the hydrogen absorption of the MH (Mg₂Ni) storage [186]. With this technique, air as the HTF was injected through multi-HTF zones of the MHHS. This study proved that higher loading pressure and airflow Re resulted in faster absorption rate. In addition, the lower inlet temperature of the HTF led to a faster absorption rate instead. Reduction in the inlet temperature of the fluid was the most effective case for improving the absorption rate. However, a study by Wang et al. [102] indicated that changing the particle size of MH material had a lesser effect on the hydrogen sorption rate.

The specific heating power also plays an important role as an evaluation indicator to provide the average power output of the system. This parameter has been applied to several thermal storage applications, including heat transformers [196], heat pumps [197], and thermal batteries [198]. The sensitivity analysis was performed under various ranges of operating parameters for the absorption process by Mou et al. [199]. These included the hydrogen supply pressure, thermal resistance between the MH and the heat exchanger, HTF flow rate and temperature. The MHHS in this study contained the helical coil tube and LaNi₅ as the MH powder. Table 9 summarises the results of this study.

Table 9. Summary of the effect of operating parameters on specific heating power from Mou et al. [199].

Parameter	Operating Range	Specific Heating Power Range (W·kg ⁻¹)	Improvement in Specific Heating Power (%)
Supply pressure	0.8–1.6 MPa	125–209	40%
Heat transfer fluid temperature	285–301 K	143–199	28%
Heat transfer fluid flow rate	18–42 L/h	166–173	4%
Thermal resistance	600–1400 mm ² ·K/W	158–186	15%

As per Table 9, the hydrogen supply pressure significantly affects specific heating power. There is a 40% improvement in the specific heating power when increasing the

supply pressure from 0.8 to 1.6 MPa, while there is only a 4% improvement in the specific heating power with the flow rate ranging between 18 and 42 L/h. The specific heating power only improves by 28% and 15% when changing HTF temperature from 285 K to 301 K and thermal resistance from $600 \text{ mm}^2 \cdot \text{K/W}$ to $1400 \text{ mm}^2 \cdot \text{K/W}$, respectively.

For comparison purposes, Figure 18 demonstrates the improvement in hydrogen sorption duration based on various operating conditions that are taken from Tables 7 and 8. The improvement in hydrogen absorption is only 11–24% when changing the initial temperature of the MHHS, while there is around 13–50% improvement in hydrogen absorption with the different ranges of flow rate and the Re of the HTF. However, the minimum improvement in hydrogen absorption by changing the hydrogen supply pressure is 20%, while the minimum improvement in the absorption by changing the HTF temperature is only 13%. In addition, with these two parameters, the maximum improvement in hydrogen absorption is 72%. It can be summarised that the hydrogen pressure and initial HTF temperature are the main parameters that significantly influence MH storage performance for the absorption process compared to the other two parameters. In contrast, the maximum improvement in hydrogen desorption based on the HTF temperature is 10 % higher than in the cases with supply pressure. The minimum improvements of desorption duration for HTF temperature and supply pressure are 20% and 15%, respectively. For the desorption process, the maximum improvement in this process based on the flow rate is 19%.

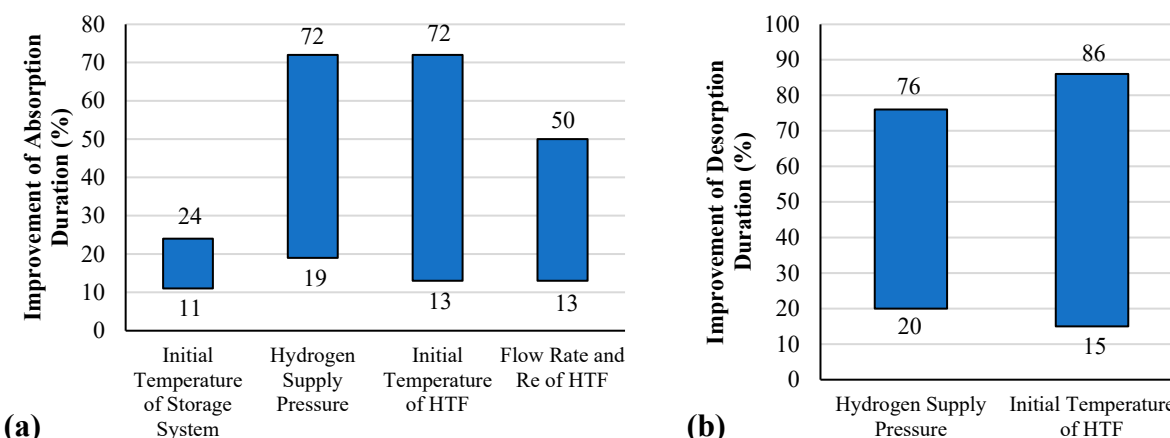


Figure 18. Improvement in hydrogen sorption duration based on various operating conditions: (a) Hydrogen absorption and (b) Hydrogen desorption.

It should be noted that the difference in improvement percentage might be because of the difference in selected operating ranges for each operating parameter. However, changing the supply pressure can positively and negatively affect the total mass absorbed [107]. Therefore, an appropriate selection of supply pressure should be considered for each new MH storage application. Moreover, in reality, there is a limitation of the initial value of the HTF inlet temperature during the cyclic application as well as during the hydrogen sorption process.

5. Application Requirements and Economic Assessments for Metal Hydride Hydrogen Storage

Most recent studies have been focused on the investigation of MHHS performance with the use of several heat exchanger types, including simple heat exchangers and complex heat exchangers. However, these studies mostly focus on small-scale hydrogen storage for both experimental and numerical works. There is only 37% of the current studies focused on large-scale systems, while the rest of the current studies focus on small-scale systems [200]. In general, small-scale experiments offer lower cost, lower safety risk, and

shorter experiment time with high flexibility compared to large-scale experiments. In other words, small-scale experiments are ideal for initial testing, feasibility studies, and concept validation. However, these experiments present lesser data accuracy and low operational complexity compared to large-scale experiments. Therefore, large-scale experiments are important for validating real-world applicability, long-term performance, and system integration. Similarly, small-scale numerical works such as CFD simulations are ideal for initial testing, conceptual designs, and fast analysis, while these simulations require lower computational costs. On the other hand, large-scale simulations offer more realistic, detailed insights that are important for commercial-scale MHHS.

As per these recent studies, all the heat exchanger types positively affect the hydrogen kinetics reaction due to the improvement in heat transfer performance inside the MHHS. However, the results can be changed when these heat exchangers are used in large-scale applications. When applying the external heat exchanger such as a cooling jacket to large-scale MHHS, this technique can cause hot spots inside the MHHS as the heat only transfers between the walls of the MH bed [15]. With the use of internal heat exchangers, the heat transfer coefficient and HTF temperature are the two main parameters that significantly affect heat transfer performance in small-scale applications. This is due to the fact that the heat directly transfers from the core of the MH bed to the wall of the HTF tube without much thermal resistance [75,201]. However, when having large-scale hydrogen storage, the amount of MH is significantly larger than in the case with small-scale hydrogen storage. The ability of the heat exchangers from the small-scale application may not be effective enough to transfer the heat. Therefore, increasing the cooling tube number is another option to increase heat transfer performance for use in large-scale applications [133]. Considering real-world applications, this technique is only recommended for cases with several straight internal tubes, not for complex heat exchanger tubes. For the use of a complex heat exchanger tube, this can be combined with other external heat exchangers such as a cooling jacket or PCM. Furthermore, improvement in thermal conductivity of the MH bed might be another option in large-scale applications instead of using complex heat exchangers. This can be achieved by several techniques such as adding metal foam or a network of fins [133,136]. However, adding metal foam might be the better option for this improvement as metal foam is more uniformly distributed within the MH compared to a network of fins [137].

In regard to the mobile and stationary applications, the primary driving factor when considering economic assessments is costs. These include the cost of raw materials and manufacturing costs including potential enhancements, quality control, recycling, target profit margins, and others [202]. However, the scale of production/application is the main aspect that significantly affects these costs, especially the manufacturing costs [203]. For the stationary MHHS, this storage always obtains higher energy density compared to the mobile MHHS. However, it requires a significantly higher cost, especially when having multiple heat exchangers or other additional equipment.

For the key trade-offs between the energy density, weight, and cost for the MHHS, the MH materials offer high volumetric energy density compared to other hydrogen storage types such as compressed gas. However, the MH materials are usually heavy, which directly increases the overall weight of the MHHS. To achieve higher energy density, specific MH materials with unique properties are required. In contrast, these specific MH materials are rare earth metals, leading to high costs. Raw material cost depends on production costs which could vary depending on abundance and form of the material occurring in nature. Some common materials used for MH are provided in Table 10.

Table 10. Material used for metal hydride and its environmental factor [203,204].

Material for MH	Abundance	Most Common Forms in Nature	Extraction/Production Method of Pure Form
Al	3rd most abundant in Earth's crust	Bauxite ore	Hall–Heroult process
Fe	4th most abundant in Earth's crust	Minerals—hematite, magnetite, siderite, banded iron formations	Reduction with coke in blast furnace followed by oxidation with air
Na	6th most abundant in Earth's crust	Minerals—NaCl, natron	Electrolysis of molten NaCl
Mg	7th most abundant in Earth's crust	Magnesite, dolomite, brucite, other minerals	Seawater, silicothermic Pidgeon process
Ti	9th most abundant in Earth's crust	Oxides in igneous rock, sediments	Kroll process
Mn	12th most abundant in Earth's crust	Pyrolusite, braunite, psilomelane	Leaching manganese ore with sulphuric acid followed by an electrowinning process
Ni	23rd most abundant in Earth's crust	Combination with sulphur and iron, laterite ore and magmatic sulphide deposits	Extractive metallurgy, conventional roasting and reduction methods
La	28th most abundant in Earth's crust	Rare earth minerals together with other lanthanides	Difficult, time consuming, and expensive multistep processes
Li	32nd most abundant in Earth's crust	Igneous rocks, granitic pegmatites, lithium salts in mineral springs and brine pools, etc.	Brine extraction, filtration of leachates in geothermal wells, mining ore

However, the key trade-offs between energy density, weight, and cost for small-scale and large-scale applications as well as the mobile and stationary applications depend on the requirements for each application. To understand these factors, extensive data from the manufacturers for each storage application are required. In general, the manufacturing costs totally depend on the production process/synthesis method and the scale of production. Regarding production methods, important factors include equipment, production time, and costs for additional materials. In some cases, several materials require production steps with high energy demand for ball milling, harsh conditions, long production times, as well as expensive dopants and catalysts to improve the MHHS properties to reach acceptable quality [203].

The potential degradation of MHs is one of the main factors that affect cyclic loading in the long-term stability of metal hydrides, leading to a decrease in overall MHHS performance. This is due to the difference in the specific volume between a high-thermal-conductivity metallic and MH powder during the hydrogen absorption/desorption cycles. Under different operating temperatures and pressures during the cycling processes, the MH powder frequently experiences expansion and contraction when repeating these cycles. This might result in a decrease in hydrogen storage capacity, swelling, loss of compactness, or crystal cracks [15,205–208]. However, different MH materials have their own different characteristics, including cyclic loading in long-term stability. Table 11 presents the advantages and disadvantages of some common MH materials. These advantages/disadvantages mainly focus on cycling stability.

Table 11. Advantages and disadvantages of metal hydride materials [203,209].

MH	Advantages	Disadvantages
LaNi ₅	<ul style="list-style-type: none"> - High volumetric capacity - Good cycling stability - High resistance towards gas impurities - Low operating temperature and pressure 	<ul style="list-style-type: none"> - Low specific energy density - Low hydrogen storage capacity at 1.4 wt% - High cost - Not abundant: rare Earth material - Flammable
Mg ₂ Ni	<ul style="list-style-type: none"> - Inexpensive and abundant - Long-term cycling without the degradation of storage capacity throughout the 1000 cyclic testing - High hydrogen storage capacity at 3.6 wt% 	<ul style="list-style-type: none"> - Slow hydrogen kinetics - High operating conditions
TiFe	<ul style="list-style-type: none"> - Inexpensive and abundant - Simple enhancement by substitution common - Good cycling stability at low pressure - Good recyclability - Mild operating conditions 	<ul style="list-style-type: none"> - Demanding conditions for (first) activation under vacuum - Relatively low gravimetric storage capacity - High sensitivity toward gas impurities and oxygen
TiMn ₂	<ul style="list-style-type: none"> - Inexpensive and abundant - Long-term stability/durability - Ambient operation temperature - Mild operating conditions 	<ul style="list-style-type: none"> - Sensitivity towards gas impurities - High equilibrium pressure plateau - Hysteresis effect - Oxygen-affine

From Table 11, it is obvious that Mg₂Ni offers cost-effective and abundant MH materials. It also offers a high hydrogen storage capacity of 3.6 wt%. However, the main disadvantages of this material are high operating conditions and slow hydrogen reaction kinetics. Other materials such as TiFe, TiMn₂, and LaNi₅ have favourable operating condition at near ambient temperatures and low pressures. However, these materials have low gravimetric energy density. Therefore, these materials are more suitable to use with stationary applications. Considering the cost of these materials, LaNi₅ is more expensive than the other two materials as La is a rare earth material. In contrast, TiFe and TiMn₂ require slightly higher operating conditions to activate the system compared to LaNi₅. However, in terms of durability, Mg₂Ni, LaNi₅, TiFe, and TiMn₂ offer good cycle stability.

6. Conclusions

Appropriate selection of MH materials, initial operating conditions of the MHHS and HTF, as well as the design and optimisation of MHHS configurations are the key factors which can positively or negatively affect the overall MHHS performance in both mobile and stationary applications. Based on these key factors, several techniques have been applied to improve the overall MHHS performance for both applications. The hydrogen absorption/desorption reaction is usually the key parameter that has been considered for the overall MHHS enhancement as MH materials basically have low thermal conductivity, resulting in slow hydrogen reaction kinetics. Therefore, a comprehensive understanding of the relationship between these key factors and the hydrogen reaction kinetics for absorption/desorption is significant to obtain suitable MHHS performance for all related applications. The main techniques that have been recently used to enhance the overall MHHS performance must be reviewed and up to date. Therefore, the key findings from this review paper are summarised as follows:

- Metal hydride materials
 - Mg-based alloys such as Mg₂Ni have high hydrogen storage capacity, light weight, and low cost, but they have low effective thermal conductivity. Intermetallic

- compounds such as La-based and Ti-based alloys have high effective thermal conductivity, but they have low hydrogen storage capacity.
- The volumetric and gravimetric density, effective thermal conductivity, and cost of MH materials should be optimised to meet the overall requirements of mobile/stationary storage applications.
 - Heat exchanger configurations
 - The well arrangement/layout of the heat exchanger structure is the key factor to increase heat transfer distribution inside the storage system. However, some limitations for manufacturing are likely in reality as most studies are based on numerical simulations.
 - The complex HTF tube structure obtains superior heat transfer performance compared to other heat exchangers. The complex HTF tube structure should be well designed and optimised to prevent huge pressure loss from the tube inlet throughout the tube outlet and maintain the system's efficiency.
 - The heat exchangers' characteristics are important for heat transfer enhancement. The coil pitch and diameter/radius are the key parameters for helical coil performance, while the number of fins and fin diameter/thickness are the main parameters for fin performance.
 - Appropriate design and optimisation of the MHHS configuration is the key factor when combining the MHHS with various heat exchanger types. The design and optimisation should be based on the gravimetric and volumetric parameters of the MHHS for each specific application.
 - When considering the gravimetric and volumetric parameters of the MHHS for mobile/stationary applications, passive heat exchanger types such as fins or PCM should be integrated with the HTF tube to improve the heat and mass transfer as well as reduce the overall storage weight.
 - When combining the PCM with other heat exchanger types, the proportional PCM/MH/HTF tube volume should be prioritised for improvement in hydrogen reaction kinetics.
 - Operating conditions
 - The hydrogen supply pressure and the HTF temperature are the main parameters for improvement in hydrogen absorption/desorption reaction compared to other parameters. To avoid the reduction in total mass absorbed, appropriate selection of supply pressure should be prioritised and well studied for each new MHSS configuration/application.
 - The HTC between the MH and HTF has a minor effect on the hydrogen sorption reaction for most MHHS types. The suitable value of the heat transfer coefficient is 500 W/mK with the use of La- and Mg-based alloys for both internal and external heat exchangers.
 - Changing the supply pressure significantly improves specific heating power by 40%, while other parameters result in less than a 30% improvement in specific heating power.

7. Limitation and Recommendation for Further Work

Considering the selection of MH materials for the use of both mobile and stationary storage applications, Mg-based alloys might be one of the good options for the MHHS due to their several advantages. To improve the hydrogen reaction kinetics and overall MHHS performance, the heat exchanger should be well designed and optimised instead.

For MHHS configurations, most studies to date have only focused on improving the heat and mass transfer performance inside the MHHS by using various heat exchanger configurations. However, these studies do not consider the relationship between the volume of the heat exchanger/MH and the hydrogen reaction kinetic. To meet the requirement of the MHHS in mobile and stationary applications, future studies should prioritise the comprehensive comparison/combination between various heat exchanger types based on the relationship between the gravimetric/volumetric parameters of the MHHS and faster hydrogen absorption/desorption reactions.

The pressure losses and fluid flow oscillation from complex heat exchangers are also the key parameters that can positively or negatively affect the overall MHHS performance. An experimental study is required to investigate the effect of these parameters on the MHHS performance for the hydrogen absorption and desorption process.

Using machine learning techniques is also one of the most effective ways to investigate MHHS performance. For MHHS applications, machine learning is only applied for the investigation of MH materials' properties. Therefore, this technique can be applied to design and optimise the overall storage performance under heat exchanger design configurations and other related factors.

Under passive and active thermal management methods, the current work only focuses on the effect of passive and active thermal management methods on the improvement in the heat transfer performance as well as the hydrogen reaction kinetics. Further evaluation of these methods in relation to the cost effectiveness as well as the energy efficiency is recommended for future work.

Due to the main objective of this work being the overall MHHS performance based on hydrogen reaction kinetics, further investigation of the degradation of MH materials as well as long-term stability due to these materials should be conducted. The more in-depth studies should also focus on the potential degradation of MH materials and its effect on the cyclic loading in long-term stability when repeating the hydrogen absorption/desorption cycles.

It is worth mentioning that there is a limitation to investigating the relationship between energy density, weight, and cost in mobile and stationary applications. The key trade-offs between energy density, weight, and cost for the MHHS usually depend on the specific requirements for each application. Extensive data from manufacturers for each storage application are required to evaluate these factors.

The heat transfer limitations in MH materials are one of the important factors that directly affect hydrogen reaction kinetics as well as the overall MHHS performance. This mainly depends on the thermal–physical properties of each MH material, which mostly have low thermal conductivity. Future studies should consider the enhancement of the thermal–physical properties of the MH materials as well as prioritise thermal management and design at the same time.

Funding: This research received no external funding.

Conflicts of Interest: The authors declare no conflict of interest.

Abbreviations

Abbreviations

CFD	Computational fluid dynamics
ETC	Effective thermal conductivity
HSC	Hydrogen storage capacity
HTC	Heat transfer coefficient
HTF	Heat transfer fluid
MH	Metal hydride

MHHS	Metal hydride-based hydrogen storage
ML	Machine learning
PCM	Phase change material
Nomenclature	
C_a	Absorption rate constant, s^{-1}
C_d	Desorption rate constant, s^{-1}
$\frac{dX}{dt}$	Hydrogen reaction kinetics
E_a	Activation energy for absorbtion, $J \text{ mol}^{-1}$
E_d	Activation energy for desorption, $J \text{ mol}^{-1}$
P_{eq}	Equilibrium pressure, Pa
P_{H_2}	Hydrogen pressure, Pa
P_{ref}	Reference pressure, Pa
R	Universal gas constant, $J \text{ K}^{-1} \text{ mol}^{-1}$
Re	Reynolds number
T	Temperature, K
t	time, s
X	Absorbed hydrogen amount, wt%
ΔH	Enthalpy of reaction, $J \text{ mol}^{-1}$
ΔS	Entropy of reaction, $J \text{ mol}^{-1} \text{ K}^{-1}$

References

1. Tange, M.; Maeda, T.; Nakano, A.; Ito, H.; Kawakami, Y.; Masuda, M.; Takahashi, T. Experimental study of hydrogen storage with reaction heat recovery using metal hydride in a totalised hydrogen energy utilisation system. *Int. J. Hydrogen Energy* **2011**, *36*, 11767–11776. [[CrossRef](#)]
2. Yue, M.; Lambert, H.; Pahon, E.; Roche, R.; Jemei, S.; Hissel, D. Hydrogen energy system: A critical review of technologies, applications, trends and challenges. *Renew. Sustain. Energy Rev.* **2021**, *146*, 111180. [[CrossRef](#)]
3. Hassanpourouzband, A.; Wilkinson, M.; Haszeldine, R.S. Hydrogen energy futures foraging or farming? Chemical Society Reviews. *R. Soc. Chem.* **2024**, *53*, 2258–2263. [[CrossRef](#)] [[PubMed](#)]
4. Hassanpourouzband, A.; Veshareh, M.J.; Wilkinson, M.; Nick, H.M.; Ngwenya, B.T.; Haszeldine, R.S. In situ hydrogen generation from underground fossil hydrocarbons. *Joule* **2025**, *9*, 101809. [[CrossRef](#)]
5. Dagdougui, H.; Sacile, R.; Bersani, C.; Ouammi, A. Hydrogen storage and distribution: Implementation scenarios. In *Hydrogen Infrastructure for Energy Applications*; Dagdougui, H., Sacile, R., Bersani, C., Ouammi, A., Eds.; Academic Press: Cambridge, UK, 2018; pp. 37–52.
6. Colozza, A.J. *Hydrogen Storage for Aircraft Applications Overview*; Technical Report; Analex Corp: Brook Park, OH, USA, 2002.
7. Moradi, R.; Groth, K.M. Hydrogen storage and delivery: Review of the state of the art technologies and risk and reliability analysis. *Int. J. Hydrogen Energy* **2019**, *44*, 12254–12269. [[CrossRef](#)]
8. Marnellos, G.E.; Athanasiou, C.; Makridis, S.S.; Kikkines, E.S. Integration of hydrogen energy technologies in autonomous power systems. In *Hydrogen-Based Autonomous Power Systems: Techno-Economic Analysis of the Integration of Hydrogen in Autonomous Power Systems 2008*; Springer: London, UK, 2004; pp. 23–81.
9. Sakintuna, B.; Lamari-Darkrim, F.; Hirscher, M. Metal hydride materials for solid hydrogen storage: A review. *Int. J. Hydrogen Energy* **2007**, *32*, 1121–1140. [[CrossRef](#)]
10. Jain, I.; Lal, C.; Jain, A. Hydrogen storage in Mg: A most promising material. *Int. J. Hydrogen Energy* **2010**, *35*, 5133–5144. [[CrossRef](#)]
11. Rusman, N.; Dahari, M. A review on the current progress of metal hydrides material for solid-state hydrogen storage applications. *Int. J. Hydrogen Energy* **2016**, *41*, 12108–12126. [[CrossRef](#)]
12. Chung, C.; Lin, C.S. Prediction of hydrogen desorption performance of Mg_2Ni hydride reactors. *Int. J. Hydrogen Energy* **2009**, *34*, 9409–9423. [[CrossRef](#)]
13. Wu, Z.; Yang, F.; Zhang, Z.; Bao, Z. Magnesium based metal hydride reactor incorporating helical coil heat exchanger: Simulation study and optimal design. *Appl. Energy* **2014**, *130*, 712–722. [[CrossRef](#)]
14. Zhao, W.; Yang, Y.; Bao, Z.; Dong, Y.; Zhu, Z. Methods for measuring the effective thermal conductivity of metal hydride beds: A review. *Int. J. Hydrogen Energy* **2020**, *45*, 6680–6700. [[CrossRef](#)]
15. Nguyen, H.Q.; Shabani, B. Review of metal hydride hydrogen storage thermal management for use in the fuel cell systems. *Int. J. Hydrogen Energy* **2021**, *46*, 31699–31726. [[CrossRef](#)]

16. Muthukumar, P.; Kumar, A.; Raju, N.N.; Malleswararao, K.; Rahman, M.M. A critical review on design aspects and developmental status of metal hydride based thermal machines. *Int. J. Hydrogen Energy* **2018**, *43*, 17753–17779. [[CrossRef](#)]
17. Rahnama, A.; Zepon, G.; Sridhar, S. Machine learning based prediction of metal hydrides for hydrogen storage, part I: Prediction of hydrogen weight percent. *Int. J. Hydrogen Energy* **2019**, *44*, 7337–7344. [[CrossRef](#)]
18. Mocanu, E.; Nguyen, P.H.; Gibescu, M.; Kling, W.L. Deep learning for estimating building energy consumption. *Sustain. Energy Grids Netw.* **2016**, *6*, 91–99. [[CrossRef](#)]
19. Hameed, G.; Ghafoor, M.A.; Yousaf, M.; Imran, M.; Zaman, M.; Elkamel, A.; Haq, A.; Rizwan, M.; Wilberforce, T.; Abdulkareem, M.A.; et al. Low temperature phase change materials for thermal energy storage: Current status and computational perspectives. *Sustain. Energy Technol. Assess.* **2022**, *50*, 101808. [[CrossRef](#)]
20. Hirscher, M.; Yartys, V.A.; Baricco, M.; von Colbe, J.B.; Blanchard, D.; Bowman, R.C.; Broom, D.P.; Buckley, C.E.; Chang, F.; Chen, P.; et al. Materials for hydrogen-based energy storage—Past, recent progress and future outlook. *J. Alloys Compd.* **2020**, *827*, 153548. [[CrossRef](#)]
21. Krishnayatra, G.; Tokas, S.; Kumar, R. Numerical heat transfer analysis & predicting thermal performance of fins for a novel heat exchanger using machine learning. *Case Stud. Therm. Eng.* **2020**, *21*, 100706.
22. Kim, K.; Kang, M.; Lee, G.; Jung, K.; Kharangate, C.R.; Asheghi, M.; Goodson, K.E.; Lee, H. A machine learning approach for predicting heat transfer characteristics in micro-pin fin heat sinks. *Int. J. Heat Mass Transf.* **2022**, *194*, 123087. [[CrossRef](#)]
23. Ostanek, J.K. Improving pin-fin heat transfer predictions using artificial neural networks. *J. Turbomach.* **2014**, *136*, 051010. [[CrossRef](#)]
24. Balachandar, C.; Arunkumar, S.; Venkatesan, M. Computational heat transfer analysis and combined ANN–GA optimization of hollow cylindrical pin fin on a vertical base plate. *Sadhana* **2015**, *40*, 1845–1863. [[CrossRef](#)]
25. Beigzadeh, R.; Rahimi, M.; Jafari, O.; Alsairafi, A.A. Computational fluid dynamics assists the artificial neural network and genetic algorithm approaches for thermal and flow modeling of air-forced convection on interrupted plate fins. *Numer. Heat Transf. Part A Appl.* **2016**, *70*, 546–565. [[CrossRef](#)]
26. Lee, H.; Kang, M.; Jung, K.W.; Kharangate, C.R.; Lee, S.; Iyengar, M.; Malone, C.; Asheghi, M.; Goodson, K.E.; Lee, H. An artificial neural network model for predicting frictional pressure drop in micro-pin fin heat sink. *Appl. Therm. Eng.* **2021**, *194*, 117012. [[CrossRef](#)]
27. Yu, X.; Shen, Y.; Guan, Z.; Zhang, D.; Tang, Z.; Li, W. Multi-objective optimization of ANN-based PSA model for hydrogen purification from steam-methane reforming gas. *Int. J. Hydrogen Energy* **2021**, *46*, 11740–11755. [[CrossRef](#)]
28. Vo, N.D.; Kang, J.H.; Oh, D.H.; Jung, M.Y.; Chung, K.; Lee, C.H. Sensitivity analysis and artificial neural network-based optimization for low-carbon H₂ production via a sorption enhanced steam methane reforming (SESMR) process integrated with separation process. *Int. J. Hydrogen Energy* **2021**, *47*, 820–847. [[CrossRef](#)]
29. Jiang, Y.; Zhang, G.; Wang, J.; Vaferi, B. Hydrogen solubility in aromatic/cyclic compounds: Prediction by difference machine learning techniques. *Int. J. Hydrogen Energy* **2021**, *46*, 23591–23602. [[CrossRef](#)]
30. Witman, M.; Ling, S.; Grant, D.M.; Walker, G.S.; Agarwal, S.; Stavila, V.; Allendorf, M.D. Extracting an empirical intermetallic hydride design principle from limited data via interpretable machine learning. *J. Phys. Chem. Lett.* **2020**, *11*, 40–47. [[CrossRef](#)]
31. Sun, K.; Esnaola, I.; Okorie, O.; Charnley, F.; Moreno, M.; Tiwari, A. Data-driven modeling and monitoring of fuel cell performance. *Int. J. Hydrogen Energy* **2021**, *46*, 33206–33217. [[CrossRef](#)]
32. Guarino, A.; Spagnuolo, G. Automatic features extraction of faults in PEM fuel cells by a Siamese artificial neural network. *Int. J. Hydrogen Energy* **2021**, *46*, 34854–34866. [[CrossRef](#)]
33. Suwarno, S.; Dicky, G.; Suyuthi, A.; Effendi, M.; Witantyo, W.; Noerochim, L.; Ismail, M. Machine learning analysis of alloying element effects on hydrogen storage properties of AB₂ metal hydrides. *Int. J. Hydrogen Energy* **2022**, *47*, 11938–11947. [[CrossRef](#)]
34. Rahnama, A.; Zepon, G.; Sridhar, S. Machine learning based prediction of metal hydrides for hydrogen storage, part II: Prediction of material class. *Int. J. Hydrogen Energy* **2019**, *44*, 7345–7353. [[CrossRef](#)]
35. Lundin, C.E.; Lynch, F.E.; Magee, C.B. A correlation between the interstitial hole sizes in intermetallic compounds and the thermodynamic properties of the hydrides formed from those compounds. *J. Less Common Met.* **1977**, *56*, 19–37. [[CrossRef](#)]
36. Mendelsohn, M.H.; Gruen, D.M.; Dwight, A.E. The effect of aluminum additions on the structural and hydrogen absorption properties of AB₅ alloys with particular reference to the LaNi₅-xAl_x ternary alloy system. *J. Less Common Met.* **1979**, *63*, 193–207. [[CrossRef](#)]
37. Reilly, J.J.; Adzic, G.D.; Johnson, J.R.; Vogt, T.; Mukerjee, S.; McBreen, J. The correlation between composition and electrochemical properties of metal hydride electrodes. *J. Alloys Compd.* **1999**, *293–295*, 569–582. [[CrossRef](#)]
38. DOE: US Department of Energy. Metal Hydride Storage Materials: Hydrogen and Fuel Cell Technologies Office. Available online: <https://www.energy.gov/eere/fuelcells/metal-hydride-storage-materials> (accessed on 5 January 2023).
39. Aoyagi, H.; Aoki, K.; Masumoto, T. Effect of ball milling on hydrogen absorption properties of FeTi, Mg₂Ni and LaNi₅. *J. Alloys Compd.* **1995**, *231*, 804–809. [[CrossRef](#)]

40. Corre, S.; Bououdina, M.; Fruchart, D.; Adachi, G.Y. Stabilisation of high dissociation pressure hydrides of formula La_{1-x}Ce_xNi₅ with carbon monoxide. *J. Alloys Compd.* **1998**, *275*, 99–104. [[CrossRef](#)]
41. Principi, G.; Agresti, F.; Maddalena, A.; Russo, S.L. The problem of solid state hydrogen storage. *Energy* **2009**, *34*, 2087–2091. [[CrossRef](#)]
42. Hahne, E.; Kallweit, J. Thermal conductivity of metal hydride materials for storage of hydrogen: Experimental investigation. *Int. J. Hydrogen Energy* **1998**, *23*, 107–114. [[CrossRef](#)]
43. Singh, A.K.; Singh, A.K.; Srivastava, O.N. On the synthesis of the Mg₂Ni alloy by mechanical alloying. *J. Alloys Compd.* **1995**, *227*, 63–68. [[CrossRef](#)]
44. Zaluski, L.; Zaluska, A.; Strom-Olsen, J.O. Hydrogen absorption in nanocrystalline Mg₂Ni formed by mechanical alloying. *J. Alloys Compd.* **1995**, *217*, 245–249. [[CrossRef](#)]
45. Abdellaoui, M.; Cracco, D.; Percheron-Guegan, A. Structural characterization and reversible hydrogen absorption properties of Mg₂Ni rich nanocomposite materials synthesized by mechanical alloying. *J. Alloys Compd.* **1998**, *268*, 233–240. [[CrossRef](#)]
46. Abdellaoui, M.; Mokbli, S.; Cuevas, F.; Latroche, M.; Guegan Percheron, A.; Zarrouk, H. Structural, solid-gas and electrochemical characterization of Mg₂Ni-rich and Mg_xNi_{100-x} amorphous-rich nanomaterials obtained by mechanical alloying. *Int. J. Hydrogen Energy* **2006**, *31*, 247–250. [[CrossRef](#)]
47. Vija, R.; Sundaresan, R.; Maiya, M.P.; Murthy, S.S. Comparative evaluation of Mg-Ni hydrogen absorbing materials prepared by mechanical alloying. *Int. J. Hydrogen Energy* **2005**, *30*, 501–508. [[CrossRef](#)]
48. Kojima, Y.; Kawai, Y.; Towata, S.I.; Matsunaga, T.; Shinozawa, T.; Kimbara, M. Development of metal hydride with high dissociation pressure. *J. Alloys Compd.* **2005**, *in press*. [[CrossRef](#)]
49. Aburto, A.; Orgaz, E. Ab initio structural and electronic investigation of magnetic R NiSn (R $\frac{1}{4}$ La, Ce, Pr, Nd) intermetallics and their hydrides. *Phys. Rev. B* **2007**, *75*, 045130. [[CrossRef](#)]
50. Shao, H.; Liu, T.; Wang, Y.; Xu, H.; Li, X. Preparation of Mg-based hydrogen storage materials from metal nanoparticles. *J. Alloys Compd.* **2008**, *465*, 527–533. [[CrossRef](#)]
51. Liang, G. Synthesis and hydrogen storage properties of Mg-based alloys. *J. Alloys Compd.* **2004**, *370*, 123–128. [[CrossRef](#)]
52. Friedlmeier, G.; Groll, M. *Proceedings International Symposium on Metal Hydrogen Systems, Les Diablerets, Switzerland, 25–30 August 1996*; pp. 497–507.
53. Pons, M.; Dantzer, P.; Guilleminot, J. A measurement technique and a new model for the wall heat transfer coefficient of a packed bed of (reactive) powder without gas flow. *Int. J. Heat Mass Transf.* **1993**, *36*, 2635–2646. [[CrossRef](#)]
54. Pons, M.; Dantzer, P. Determination of thermal conductivity and wall heat transfer coefficient of hydrogen storage materials. *Int. J. Hydrogen Energy* **1994**, *19*, 611–616. [[CrossRef](#)]
55. Ron, M.; Bershadsky, E.; Josephy, Y. The thermal conductivity of porous metal matrix hydride compacts. *J. Less Common Met.* **1991**, *172*, 1138–1146. [[CrossRef](#)]
56. Ishido, Y.; Kawamura, M.; Ono, S. Thermal conductivity of magnesium-nickel hydride powder beds in a hydrogen atmosphere. *Int. J. Hydrogen Energy* **1982**, *7*, 173–182. [[CrossRef](#)]
57. Suissa, E.; Jacob, I.; Hadari, Z. Experimental measurements and general conclusions on the effective thermal conductivity of powdered metal hydrides. *J. Less Common Met.* **1984**, *104*, 287–295. [[CrossRef](#)]
58. Sun, D.W.; Deng, S.J. Theoretical descriptions and experimental measurements on the effective thermal conductivity in metal hydride powder beds. *J. Less Common Met.* **1990**, *160*, 387–395.
59. Kumar, E.A.; Maiya, M.P.; Murthy, S.S. Measurement and analysis of effective thermal conductivity of MmNi_{4.5}Al_{0.5} hydride bed. *Ind. Eng. Chem. Res.* **2011**, *50*, 12990–12999. [[CrossRef](#)]
60. Christopher, M.D. *Application of the Transient Hot-Wire Technique for Measurement of Effective Thermal Conductivity of Catalyzed Sodium Alanate for Hydrogen Storage*; Virginia Tech: Blacksburg, VA, USA, 2006.
61. Dedrick, D.; Kanouff, M.; Replogle, B.; Gross, K. Thermal properties characterization of sodium alanates. *J. Alloys Compd.* **2005**, *389*, 299–305. [[CrossRef](#)]
62. Ahluwalia, R.K. Sodium alanate hydrogen storage system for automotive fuel cells. *Int. J. Hydrogen Energy* **2007**, *32*, 1251–1261. [[CrossRef](#)]
63. Flueckiger, S.; Voskuilen, T.; Pourpoint, T.; Fisher, T.S.; Zheng, Y. In situ characterization of metal hydride thermal transport properties. *Int. J. Hydrogen Energy* **2010**, *35*, 614–621. [[CrossRef](#)]
64. Goodell, P. Thermal conductivity of hydriding alloy powders and comparisons of reactor systems. *J. Less Common Met.* **1980**, *74*, 175–184. [[CrossRef](#)]
65. Kempf, A.; Martin, W. Measurement of the thermal properties of TiFe0.85Mn0.15 and its hydrides. *Int. J. Hydrogen Energy* **1986**, *11*, 107–116. [[CrossRef](#)]
66. Suda, S.; Kobayashi, N.; Yoshida, K.; Ishido, Y.; Ono, S. Experimental measurements of thermal conductivity. *J. Less Common Met.* **1980**, *74*, 127–136. [[CrossRef](#)]

67. Suda, S.; Kobayashi, N.; Yoshida, K. Thermal conductivity in metal hydride beds. *Int. J. Hydrogen Energy* **1981**, *6*, 521–528. [[CrossRef](#)]
68. Sandrock, G. A panoramic overview of hydrogen storage alloys from a gas reaction point of view. *J. Alloys Compd.* **1999**, *293–295*, 877–888. [[CrossRef](#)]
69. Sandrock, G.D. Development of low cost nickel-rare earth hydrides for hydrogen storage. In Proceedings of the 2nd World Hydrogen Energy Conference, Zurich, Switzerland, 21–24 August 1978; Veziroglu, T.N., Seifritz, W., Eds.; Pergamon: Oxford, UK, 1979; Volume 3, pp. 1625–1656.
70. Chandra, D.; Chien, W.M.; Talekar, A. Rare earths—Crucial elements of advanced technology. *Mater. Matters* **2011**, *6*, 51.
71. Sandrock, G.; Thomas, G. *Compilation of IEA/DOE/SNL Databases Technical Report for International Energy Agency (IEA)*; 1997.
72. Reilly, J.; Wiswall, R.H. Hydrogen Storage and Purification Technical Report for Brookhaven National Laboratory. 1972. Available online: <https://www.osti.gov/biblio/5291031> (accessed on 3 March 2025).
73. Sreeraj, R.; Aadhithiyan, A.K.; Anbarasu, S. Integration of thermal augmentation methods in hydride beds for metal hydride based hydrogen storage systems: Review and recommendation. *J. Energy Storage* **2022**, *52*, 105039. [[CrossRef](#)]
74. Mazzucco, A.; Dornheim, M.; Sloth, M.; Jensen, T.R.; Jensen, J.O.; Rokni, M. Bed geometries, fueling strategies and optimisation of heat exchanger designs in metal hydride storage systems for automotive applications: A review. *Int. J. Hydrogen Energy* **2014**, *39*, 17054–17074. [[CrossRef](#)]
75. Chung, C.A.; Ho, C.J. Thermal-fluid behavior of the hydriding and dehydriding processes in a metal hydride hydrogen storage canister. *Int. J. Hydrogen Energy* **2009**, *34*, 4351–4364. [[CrossRef](#)]
76. Valizadeh, M.; Aghajani Delavar, M.; Farhadi, M. Numerical simulation of heat and mass transfer during hydrogen desorption in metal hydride storage tank by Lattice Boltzmann method. *Int. J. Hydrogen Energy* **2016**, *41*, 413–424. [[CrossRef](#)]
77. Wang, Y.; Adroher, X.C.; Chen, J.; Yang, X.G.; Miller, T. Three dimensional modeling of hydrogen sorption in metal hydride hydrogen storage beds. *J. Power Sources* **2009**, *194*, 997–1006. [[CrossRef](#)]
78. Nam, J.; Ko, J.; Ju, H. Three-dimensional modeling and simulation of hydrogen absorption in metal hydride hydrogen storage vessels. *Appl. Energy* **2012**, *89*, 164–175. [[CrossRef](#)]
79. Yoo, H.; Kim, W.; Ju, H. A numerical comparison of hydrogen absorption behaviors of uranium and zirconium cobaltbased metal hydride beds. *Solid State Ionics* **2014**, *262*, 241–247. [[CrossRef](#)]
80. Patil, S.D.; Gopal, M.R. Analysis of a metal hydride reactor for hydrogen storage. *Int. J. Hydrogen Energy* **2013**, *38*, 942–951. [[CrossRef](#)]
81. Urunkar, R.U.; Patil, S.D. Enhancement of heat and mass transfer characteristics of metal hydride reactor for hydrogen storage using various nanofluids. *Int. J. Hydrogen Energy* **2021**, *46*, 19486–19497. [[CrossRef](#)]
82. Yiotis, A.G.; Kainourgiakis, M.E.; Charalambopoulou, G.C.; Stubos, A.K. A generic physical model for a thermally integrated high-temperature PEM fuel cell and sodium alanate tank system. *Int. J. Hydrogen Energy* **2015**, *40*, 14551–14561. [[CrossRef](#)]
83. Hwang, J.J.; Chang, W.R. Characteristic study on fuel cell/ battery hybrid power system on a light electric vehicle. *J. Power Sources* **2012**, *207*, 111–119. [[CrossRef](#)]
84. Weiss-Ungethum, J.; Burger, I.; Schmidt, N.; Linder, M.; Kallo, J. Experimental investigation of a liquid cooled high temperature proton exchange membrane (HT-PEM) fuel cell coupled to a sodium alanate tank. *Int. J. Hydrogen Energy* **2014**, *39*, 5931–5941. [[CrossRef](#)]
85. Wu, Z.; Yang, F.; Zhu, L.; Feng, P.; Zhang, Z.; Wang, Y. Improvement in hydrogen desorption performances of magnesium based metal hydride reactor by incorporating helical coil heat exchanger. *Int. J. Hydrogen Energy* **2016**, *41*, 16108–16121. [[CrossRef](#)]
86. Wang, D.; Wang, Y.; Huang, Z.; Yang, F.; Wu, Z.; Zheng, L. Design optimisation and sensitivity analysis of the radiation minichannel metal hydride reactor. *Energy* **2019**, *173*, 443–456. [[CrossRef](#)]
87. Anbarasu, S.; Muthukumar, P.; Mishra, S.C. Thermal modeling of $\text{LmNi}_{4.91}\text{Sn}_{0.15}$ based solid state hydrogen storage device with embedded cooling tubes. *Int. J. Hydrogen Energy* **2014**, *39*, 15549–15562. [[CrossRef](#)]
88. Bao, Z.; Wu, Z.; Nyamsi, S.N.; Yang, F.; Zhang, Z. Three-dimensional modeling and sensitivity analysis of multitubular metal hydride reactors. *Appl. Therm. Eng.* **2013**, *52*, 97–108. [[CrossRef](#)]
89. Mellouli, S.; Dhaou, H.; Askri, F.; Jemni, A.; Nasrallah, S.B. Hydrogen storage in metal hydride tanks equipped with metal foam heat exchanger. *Int. J. Hydrogen Energy* **2009**, *34*, 9393–9401. [[CrossRef](#)]
90. Raju, M.; Kumar, S. System simulation modeling and heat transfer in sodium alanate based hydrogen storage systems. *Int. J. Hydrogen Energy* **2011**, *36*, 1578–1591. [[CrossRef](#)]
91. Hardy, B.J.; Anton, D.L. Hierarchical methodology for modelling hydrogen storage systems. Part II: Detailed models. *Int. J. Hydrogen Energy* **2009**, *34*, 2992–3004. [[CrossRef](#)]
92. Bhouri, M.; Burger, I.; Linder, M. Numerical investigation of hydrogen charging performance for a combination reactor with embedded metal hydride and coolant tubes. *Int. J. Hydrogen Energy* **2015**, *40*, 6626–6638. [[CrossRef](#)]
93. Mohan, G.; Maiya, M.P.; Murthy, S.S. Performance simulation of metal hydride hydrogen storage device with embedded filters and heat exchanger tubes. *Int. J. Hydrogen Energy* **2007**, *32*, 4978–4987. [[CrossRef](#)]

94. Kumar, A.; Raju, N.N.; Muthukumar, P.; Selvan, P.V. Experimental studies on industrial scale metal hydride based hydrogen storage system with embedded cooling tubes. *Int. J. Hydrogen Energy* **2019**, *44*, 13549–13560. [[CrossRef](#)]
95. Raju, N.N.; Kumar, A.; Malleswararao, K.; Muthukumar, P. Parametric studies on LaNi_{4.7}Al_{0.3} based hydrogen storage reactor with embedded cooling tubes. *Energy Procedia* **2019**, *158*, 2384–2390. [[CrossRef](#)]
96. Singh, A.; Maiya, M.P.; Srinivasa Murthy, S. Performance of a solid state hydrogen storage device with finned tube heat exchanger. *Int. J. Hydrogen Energy* **2017**, *42*, 26855–26871. [[CrossRef](#)]
97. Singh, A.; Maiya, M.P.; Srinivasa Murthy, S. Experiments on solid state hydrogen storage device with a finned tube heat exchanger. *Int. J. Hydrogen Energy* **2017**, *42*, 15226–15235. [[CrossRef](#)]
98. Singh, A.; Maiya, M.P.; Srinivasa Murthy, S. Effects of heat exchanger design on the performance of a solid state hydrogen storage device. *Int. J. Hydrogen Energy* **2015**, *40*, 9733–9746. [[CrossRef](#)]
99. Yang, W.; Ye, Y.; Cheng, H.; Liu, J.; Yan, K.; Miao, H. Performance optimization of a U-tube heat exchanger type hydrogen storage reactor with a novel fin structure. *Int. J. Hydrogen Energy* **2025**, *82*, 272–280. [[CrossRef](#)]
100. Li, H.; Wang, Y.; He, C.; Chen, X.; Zhang, Q.; Zheng, L.; Yang, F.; Zhang, Z. Design and performance simulation of the spiral mini-channel reactor during H₂ absorption. *Int. J. Hydrogen Energy* **2015**, *40*, 13490–13505. [[CrossRef](#)]
101. Meng, X.; Wu, Z.; Bao, Z.; Yang, F.; Zhang, Z. Performance simulation and experimental confirmation of a minichannel metal hydrides reactor. *Int. J. Hydrogen Energy* **2013**, *38*, 15242–15253. [[CrossRef](#)]
102. Wang, D.; Wang, Y.; Wang, F.; Zheng, S.; Guan, S.; Zheng, L.; Wu, L.; Fang, T.; Yang, X.; Lv, M. Hydrogen storage in branch mini-channel metal hydride reactor: Optimisation design, sensitivity analysis and quadratic regression. *Int. J. Hydrogen Energy* **2021**, *46*, 25189–25207. [[CrossRef](#)]
103. Fernández, R.Á.; Caraballo, C.S.; Cilleruelo, B.F.; Lozano, J.A. Fuel optimization strategy for hydrogen fuel cell range extender vehicles applying genetic algorithms. *Renew. Sustain. Energy Rev.* **2018**, *81*, 655–668. [[CrossRef](#)]
104. Raju, M.; Kumar, S. Optimisation of heat exchanger designs in metal hydride based hydrogen storage systems. *Int. J. Hydrogen Energy* **2012**, *37*, 2767–2778. [[CrossRef](#)]
105. Shafiee, S.; McCay, M.H. Different reactor and heat exchanger configurations for metal hydride hydrogen storage systemsea review. *Int. J. Hydrogen Energy* **2016**, *41*, 9462–9470. [[CrossRef](#)]
106. Wang, H.; Prasad, A.K.; Advani, S.G. Hydrogen storage system based on hydride materials incorporating a helical-coil heat exchanger. *Int. J. Hydrogen Energy* **2012**, *37*, 14292–14299. [[CrossRef](#)]
107. Mellouli, S.; Askri, F.; Dhaou, H.; Jemni, A.; Nasrallah, S.B. A novel design of a heat exchanger for a metal-hydrogen reactor. *Int. J. Hydrogen Energy* **2007**, *32*, 3501–3507. [[CrossRef](#)]
108. Bhogilla, S.S. Design of a AB₂-metal hydride cylindrical tank for renewable energy storage. *J. Energy Storage* **2017**, *14*, 203–210. [[CrossRef](#)]
109. Visaria, M.; Mudawar, I. Coiled-tube heat exchanger for high pressure Metal Hydride hydrogen storage systemse Part 1. Experimental study. *Int. J. Heat Mass Transf.* **2012**, *55*, 1782–1795. [[CrossRef](#)]
110. Visaria, M.; Mudawar, I. Coiled-tube heat exchanger for high pressure metal hydride hydrogen storage systemse Part 2. Computational model. *Int. J. Heat Mass Transf.* **2012**, *55*, 1796–1806. [[CrossRef](#)]
111. Dong, D.; Humphries, T.D.; Sheppard, D.A.; Stansby, B.; Paskevicius, M.; Sofianos, M.V.; Chaudhary, A.L.; Dornheim, M.; Buckley, C.E. Thermal optimisation of metal hydride reactors for thermal energy storage applications. *Sustain. Energy Fuels* **2017**, *1*, 1820. [[CrossRef](#)]
112. Mathew, A.; Nadim, N.; Chandratilleke, T.T.; Humphries, T.D.; Paskevicius, M.; Buckley, C.E. Performance analysis of a hightemperature magnesium hydride reactor tank with a helical coil heat exchanger for thermal storage. *Int. J. Hydrogen Energy* **2021**, *46*, 1038–1055. [[CrossRef](#)]
113. Tiwari, S.; Sharma, P. Optimisation based methodology to design metal hydride reactor for thermal storage application. *J. Energy Storage* **2021**, *41*, 102845. [[CrossRef](#)]
114. Ardahaie, S.S.; Hosseini, M.J.; Eisapour, M.; Eisapour, A.H.; Ranjbar, A.A. A novel porous metal hydride tank for hydrogen energy storage and consumption assisted by PCM jackets and spiral tubes. *J. Clean. Prod.* **2021**, *311*, 127674. [[CrossRef](#)]
115. Eisapour, A.H.; Naghizadeh, A.; Eisapour, M.; Talebizadehsardari, P. Optimal design of a metal hydride hydrogen storage bed using a helical coil heat exchanger along with a central return tube during the absorption process. *Int. J. Hydrogen Energy* **2021**, *46*, 14478–14493. [[CrossRef](#)]
116. Wang, D.; Li, S.; Huang, Z.; Liu, Z.; Wang, Y.; Yang, F.; Wu, Z.; Zhang, Z.; Wu, J.; Shi, L.; et al. Design optimisation, sensitivity analysis and operational comparison of a duplex helical elliptical tube metal hydride reactor. *Sustain. Energy Fuels* **2020**, *4*, 5851–5868. [[CrossRef](#)]
117. Larpruenrudee, P.; Bennett, N.S.; Gu, Y.T.; Fitch, R.; Islam, M.S. Design optimization of a magnesium-based metal hydride hydrogen energy storage system. *Sci. Rep.* **2022**, *12*, 13436. [[CrossRef](#)]

118. Larpruenrudee, P.; Bennett, N.S.; Hossain, M.J.; Fitch, R.; Islam, M.S. Hydrogen energy storage system: How does the semi-cylindrical helical coil heat exchanger affect metal hydride beds' thermal conductivity? In Proceeding of the 23rd Australasian Fluid Mechanics Conference, Sydney, Australia, 4–8 December 2022; p. 421.
119. Larpruenrudee, P.; Bennett, N.S.; Luo, Z.; Fitch, R.; Sauret, E.; Islam, M.S. A novel design for faster hydrogen storage: A combined semi-cylindrical and central return tube heat exchanger. *J. Energy Storage* **2023**, *71*, 108018. [\[CrossRef\]](#)
120. Larpruenrudee, P.; Bennett, N.S.; Fitch, R.; Sauret, E.; Gu, Y.T.; Islam, M.S. Investigation of metal hydride hydrogen storage performance using phase change materials. *Int. J. Hydrogen Energy* **2024**, *60*, 996–1019. [\[CrossRef\]](#)
121. Andreasen, G.; Melnichuk, M.; Ramos, S.; Corso, H.L.; Visintin, A.; Triaca, W.E.; Peretti, H.A. Hydrogen desorption from a hydride container under different heat exchange conditions. *Int. J. Hydrogen Energy* **2013**, *38*, 13352–13359. [\[CrossRef\]](#)
122. MacDonald, B.D.; Rowe, A.M. Impacts of external heat transfer enhancements on metal hydride storage tanks. *Int. J. Hydrogen Energy* **2006**, *31*, 1721–1731. [\[CrossRef\]](#)
123. Veeraju, C.; Gopal, M.R. Heat and mass transfer studies on plate fin-and-elliptical tube type metal hydride reactors. *Appl. Therm. Eng.* **2010**, *30*, 673–682. [\[CrossRef\]](#)
124. Keshari, V.; Maiya, M.P. Design and investigation of hydriding alloy based hydrogen storage reactor integrated with a pin fin tube heat exchanger. *Int. J. Hydrogen Energy* **2018**, *43*, 7081–7095. [\[CrossRef\]](#)
125. Nyamsi, S.N.; Yang, F.; Zhang, Z. An optimisation study on the finned tube heat exchanger used in hydride hydrogen storage system-analytical method and numerical simulation. *Int. J. Hydrogen Energy* **2012**, *37*, 16078–16092. [\[CrossRef\]](#)
126. Keshari, V.; Maiya, M.P. Numerical study of solid state hydrogen storage system with finned tube heat exchanger. *Heat Transf. Eng.* **2020**, *41*, 484–496. [\[CrossRef\]](#)
127. Garrison, S.L.; Hardy, B.J.; Gorbounov, M.B.; Tamburello, D.A.; Cognale, C.; Mosher, D.A.; Anton, D.L. Optimisation of internal heat exchangers for hydrogen storage tanks utilising metal hydrides. *Int. J. Hydrogen Energy* **2012**, *37*, 2850–2861. [\[CrossRef\]](#)
128. Muthukumar, P.; Singhal, A.; Bansal, G. Thermal modeling and performance analysis of industrial-scale metal hydride based hydrogen storage container. *Int. J. Hydrogen Energy* **2012**, *37*, 14351–14364. [\[CrossRef\]](#)
129. Krishna, K.V.; Kanti, P.K.; Maiya, M.P. A novel fin efficiency concept to optimize solid state hydrogen storage reactor. *Energy* **2024**, *288*, 129789. [\[CrossRef\]](#)
130. Mellouli, S.; Abhilash, E.; Askri, F.; Nasrallah, S.B. Integration of thermal energy storage unit in a metal hydride hydrogen storage tank. *Appl. Therm. Eng.* **2016**, *102*, 1185–1196. [\[CrossRef\]](#)
131. Alqahtani, T.; Mellouli, S.; Bamasag, A.; Askri, F.; Phelan, P.E. Thermal performance analysis of a metal hydride reactor encircled by a phase change material sandwich bed. *Int. J. Hydrogen Energy* **2020**, *45*, 23076–23092. [\[CrossRef\]](#)
132. Alqahtani, T.; Mellouli, S.; Bamasag, A.; Askri, F.; Phelan, P.E. Cyclic behaviors of a novel design of a metal hydride reactor encircled by cascaded phase change materials. *Int. J. Hydrogen Energy* **2020**, *45*, 32285–32297. [\[CrossRef\]](#)
133. Afzal, M.; Sharma, P. Design of a large-scale metal hydride based hydrogen storage reactor: Simulation and heat transfer optimisation. *Int. J. Hydrogen Energy* **2018**, *43*, 13356–13372. [\[CrossRef\]](#)
134. Minko, K.B.; Artemov, V.I.; Yan'Kov, G.G. Numerical study of hydrogen purification using metal hydride reactor with aluminium foam. *Appl. Therm. Eng.* **2015**, *76*, 175–184. [\[CrossRef\]](#)
135. Suda, S. Recent development of hydride energy systems in Japan. *Int. J. Hydrogen Energy* **1985**, *10*, 757–765. [\[CrossRef\]](#)
136. Laurencelle, F.; Goyette, J. Simulation of heat transfer in a metal hydride reactor with aluminium foam. *Int. J. Hydrogen Energy* **2007**, *32*, 2957–2964. [\[CrossRef\]](#)
137. Ferekh, S.; Gwak, G.; Kyoung, S.; Kang, H.; Chang, M.; Yun, S.; Oh, Y.-H.; Kim, W.; Kim, D.; Hong, T.; et al. Numerical comparison of heat-fin-and-metal-foam-based hydrogen storage beds during hydrogen charging process. *Int. J. Hydrogen Energy* **2015**, *40*, 1440–1450. [\[CrossRef\]](#)
138. Darzi, A.A.R.; Afrouzi, H.H.; Moshfegh, A.; Farhadi, M. Absorption and desorption of hydrogen in long metal hydride tank equipped with phase change material jacket. *Int. J. Hydrogen Energy* **2016**, *41*, 9595–9610. [\[CrossRef\]](#)
139. Kalbasi, R. Introducing a novel heat sink comprising PCM and air-adapted to electronic device thermal management. *Int. J. Heat Mass Transf.* **2021**, *169*, 120914. [\[CrossRef\]](#)
140. Ren, Q.; Guo, P.; Zhu, J. Thermal management of electronic devices using pin-fin based cascade microencapsulated PCM/expanded graphite composite. *Int. J. Heat Mass Transf.* **2020**, *149*, 119199. [\[CrossRef\]](#)
141. Adilkhanova, I.; Memon, S.A.; Kim, J.; Sheriyev, A. A novel approach to investigate the thermal comfort of the lightweight relocatable building integrated with PCM in different climates of Kazakhstan during summertime. *Energy* **2021**, *217*, 119390. [\[CrossRef\]](#)
142. Qu, Y.; Zhou, D.; Xue, F.; Cui, L. Multi-factor analysis on thermal comfort and energy saving potential for PCM-integrated buildings in summer. *Energy Build.* **2021**, *241*, 110966. [\[CrossRef\]](#)
143. Ling, Z.; Zhang, Z.; Shi, G.; Fang, X.; Wang, L.; Gao, X.; Fang, Y.; Xu, T.; Wang, S.; Liu, X. Review on thermal management systems using phase change materials for electronic components, Li-ion batteries and photovoltaic modules. *Renew. Sustain. Energy Rev.* **2014**, *31*, 427–438. [\[CrossRef\]](#)

144. Cui, Y.; Zeng, X.; Xiao, J.; Kou, H. The comprehensive review for development of heat exchanger configuration design in metal hydride bed. *Int. J. Hydrogen Energy* **2022**, *47*, 2461–2490. [[CrossRef](#)]
145. Nyamsi, S.N.; Tolj, I.; Lotoskyy, M. Metal hydride beds-phase change materials, dual mode thermal energy storage for medium-high temperature industrial waste heat recovery. *Energies* **2019**, *12*, 3949. [[CrossRef](#)]
146. Tong, L.; Xiao, J.; B'enard, P.; Chahine, R. Thermal management of metal hydride hydrogen storage reservoir using phase change materials. *Int. J. Hydrogen Energy* **2019**, *44*, 21055–21066. [[CrossRef](#)]
147. Tong, L.; Yuan, Y.; Yang, T.; Benard, P.; Yuan, C.; Xiao, J. Hydrogen release from a metal hydride tank with phase change material jacket and coiled-tube heat exchanger. *Int. J. Hydrogen Energy* **2021**, *46*, 32135–32148. [[CrossRef](#)]
148. Yao, J.; Zhu, P.; Guo, L.; Duan, L.; Zhang, Z.; Kurko, S.; Wu, Z. A continuous hydrogen absorption/desorption model for metal hydride reactor coupled with PCM as heat management and its application in the fuel cell power system. *Int. J. Hydrogen Energy* **2020**, *45*, 28087–28099. [[CrossRef](#)]
149. El Mghari, H.; Huot, J.; Tong, L.; Xiao, J. Selection of phase change materials, metal foams and geometries for improving metal hydride performance. *Int. J. Hydrogen Energy* **2020**, *45*, 14922–14939. [[CrossRef](#)]
150. El Mghari, H.; Huot, J.; Xiao, J. Analysis of hydrogen storage performance of metal hydride reactor with phase change materials. *Int. J. Hydrogen Energy* **2019**, *44*, 28893–28908. [[CrossRef](#)]
151. Lewis, S.D.; Chippar, P. Analysis of heat and mass transfer during charging and discharging in a metal hydride-phase change material reactor. *J. Energy Storage* **2021**, *33*, 102108. [[CrossRef](#)]
152. Maad, H.B.; Askri, F.; Nasrallah, S.B. Heat and mass transfer in a metal hydrogen reactor equipped with a phase-change heat-exchanger. *Int. J. Therm. Sci.* **2016**, *99*, 271–278. [[CrossRef](#)]
153. Maad, H.B.; Miled, A.; Askri, F.; Nasrallah, S.B. Numerical simulation of absorption-desorption cyclic processes for metal-hydrogen reactor with heat recovery using phasechange material. *Appl. Therm. Eng.* **2016**, *96*, 267–276. [[CrossRef](#)]
154. Garrier, S.; Delhomme, B.; De Rango, P.; Marty, P.; Fruchart, D.; Miraglia, S. A new MgH₂ tank concept using a phase-change material to store the heat of reaction. *Int. J. Hydrogen Energy* **2013**, *38*, 9766–9771. [[CrossRef](#)]
155. Mellouli, S.; Khedher, N.B.; Askri, F.; Jemni, A.; Nasrallah, S.B. Numerical analysis of metal hydride tank with phase change material. *Appl. Therm. Eng.* **2015**, *90*, 674–682. [[CrossRef](#)]
156. Mellouli, S.; Askri, F.; Abhilash, E.; Nasrallah, S.B. Impact of using a heat transfer fluid pipe in a metal hydride-phase change material tank. *Appl. Therm. Eng.* **2017**, *113*, 554–565. [[CrossRef](#)]
157. Nguyen, H.Q.; Shabani, B. Metal hydride thermal management using phase change material in the context of a standalone solar-hydrogen system. *Energy Convers. Manag.* **2020**, *224*, 113352. [[CrossRef](#)]
158. Ye, Y.; Lu, J.; Ding, J.; Wang, W.; Yan, J. Numerical simulation on the storage performance of a phase change materials based metal hydride hydrogen storage tank. *Appl. Energy* **2020**, *278*, 115682. [[CrossRef](#)]
159. Maad, H.B.; Askri, F.; Virgone, J.; Nasrallah, S.B. Numerical study of high temperature metal-hydrogen reactor (Mg₂Ni-H₂) with heat reaction recovery using phase change material during desorption. *Appl. Therm. Eng.* **2018**, *140*, 225–234. [[CrossRef](#)]
160. Dai, H.; Chen, Z.; Cao, H.; Tian, Z.; Zhang, M.; Wang, X.; He, S.; Wang, W.; Gao, M. Effect of partition arrangement of metal hydrides and phase change materials on hydrogen absorption performance in the metal hydride reactor. *Int. J. Hydrogen Energy* **2024**, *84*, 780–792. [[CrossRef](#)]
161. Ye, Y.; Ding, J.; Wang, W.; Yan, J. The storage performance of metal hydride storage tanks with reaction heat recovery by phase change materials. *Appl. Energy* **2021**, *299*, 117255. [[CrossRef](#)]
162. Ye, Y.; Yue, Y.; Lu, J.; Ding, J.; Wang, W.; Yan, J. Enhanced hydrogen storage of a LaNi₅ based reactor by using phase change materials. *Renew. Energy* **2021**, *180*, 734–743. [[CrossRef](#)]
163. Bai, X.S.; Yang, W.W.; Tang, X.Y.; Yang, F.S.; Jiao, Y.H.; Yang, Y. Optimisation of tree-shaped fin structures towards enhanced absorption performance of metal hydride hydrogen storage device: A numerical study. *Energy* **2021**, *220*, 119738. [[CrossRef](#)]
164. Souahlia, A.; Dhaou, H.; Mellouli, S.; Askri, F.; Jemni, A.; Nasrallah, S.B. Experimental study of metal hydride-based hydrogen storage tank at constant supply pressure. *Int. J. Hydrogen Energy* **2014**, *39*, 7365–7372. [[CrossRef](#)]
165. Ma, J.; Wang, Y.; Shi, S.; Yang, F.; Bao, Z.; Zhang, Z. Optimisation of heat transfer device and analysis of heat & mass transfer on the finned multi-tubular metal hydride tank. *Int. J. Hydrogen Energy* **2014**, *39*, 13583–13595.
166. Mallik, A.; Sharma, P. Modeling and numerical simulation of an industrial scale metal hydride reactor based on CFD-Taguchi combined method. *Energy Storage* **2021**, *3*, 227. [[CrossRef](#)]
167. Liu, Y.; Wang, H.; Ayub, I.; Yang, F.; Wu, Z.; Zhang, Z. A variable cross-section annular fins type metal hydride reactor for improving the phenomenon of inhomogeneous reaction in the thermal energy storage processes. *Appl. Energy* **2021**, *295*, 117073. [[CrossRef](#)]
168. Ayub, I.; Nasir, M.S.; Liu, Y.; Munir, A.; Wu, Z.; Yang, F.; Zhang, Z. Numerical modeling and performance comparison of high-temperature metal hydride reactor equipped with bakery system for solar thermal energy storage. *Int. J. Hydrogen Energy* **2020**, *45*, 31612–31631. [[CrossRef](#)]

169. Krishna, K.B.; Kanti, P.K.; Maiya, M.P. Design optimization of metal hydride-based hydrogen storage reactor using fin efficiency concept. In Proceedings of the 38th ISTANBUL International Conference on Advances in "Science, Engineering & Technology" (IASET-24), Istanbul, Turkiye, 13–15 May 2024.
170. Dhaou, H.; Ben Khedher, N.; Mellouli, S.; Souahlia, A.; Askri, F.; Jemni, A.; Ben Nasrallah, S. Improvement of thermal performance of spiral heat exchanger on hydrogen storage by adding copper fins. *Int. J. Therm. Sci.* **2011**, *50*, 2536–2542. [\[CrossRef\]](#)
171. Mellouli, S.; Askri, F.; Dhaou, H.; Jemni, A.; Nasrallah, S.B. Numerical simulation of heat and mass transfer in metal hydride hydrogen storage tanks for fuel cell vehicles. *Int. J. Hydrogen Energy* **2010**, *35*, 1693–1705. [\[CrossRef\]](#)
172. Krishna, K.V.; Kanti, P.K.; Maiya, M.P. A novel flat coil tube heat exchanger for metal hydride hydrogen storage reactors. *Int. J. Hydrogen Energy* **2024**, *64*, 98–108. [\[CrossRef\]](#)
173. Freni, A.; Cipiti, F.; Cacciola, G. Finite element-based simulation of a metal hydride-based hydrogen storage tank. *Int. J. Hydrogen Energy* **2009**, *34*, 8574–8582. [\[CrossRef\]](#)
174. Karmakar, A.; Mallik, A.; Gupta, N.; Sharma, P. Studies on 10kg alloy mass metal hydride based reactor for hydrogen storage. *Int. J. Hydrogen Energy* **2021**, *46*, 5495–5506. [\[CrossRef\]](#)
175. Shtivastav, A.P.; Kanti, P.K.; Mohan, G.; Maiya, M.P. Design and optimization of metal hydride reactor with phase change material using fin factor for hydrogen storage. *J. Energy Storage* **2024**, *77*, 109975. [\[CrossRef\]](#)
176. Kaplan, Y. Effect of design parameters on enhancement of hydrogen charging in metal hydride reactors. *Int. J. Hydrogen Energy* **2009**, *34*, 2288–2294. [\[CrossRef\]](#)
177. Tong, L.; Xiao, J.; Yang, T.; B'enard, P.; Chahine, R. Complete and reduced models for metal hydride reactor with coiled-tube heat exchanger. *Int. J. Hydrogen Energy* **2019**, *44*, 15907–15916. [\[CrossRef\]](#)
178. Askri, F.; Salah, M.B.; Jemni, A.; Nasrallah, S.B. Optimisation of hydrogen storage in metal-hydride tanks. *Int. J. Hydrogen Energy* **2009**, *34*, 897–905. [\[CrossRef\]](#)
179. Sekhar, B.S.; Lototskyy, M.; Kolesnikov, A.; Moropeng, M.L.; Tarasov, B.; Pollet, B. Performance analysis of cylindrical metal hydride beds with various heat exchange options. *J. Alloys Compd.* **2015**, *645*, S89–S95. [\[CrossRef\]](#)
180. Zheng, S.; Wang, Y.; Wang, D.; Guan, S.; Liu, Y.; Wang, F.; Zheng, L.; Wu, L.; Gao, X.; Zhang, Z. Design and performance study on the primary & secondary helical-tube reactor. *Energy* **2023**, *263*, 125840.
181. Guan, F.; Ma, W.; Tu, Y.; Zhou, C.; Zhou, B. An experimental study of flow behavior of coiled tubing drilling system. *Adv. Mech. Eng.* **2014**, *6*, 935159. [\[CrossRef\]](#)
182. Zhang, Z.; Liu, H. Research on the thermal performance of a helical coil heat exchanger. In Proceedings of the International Conference of Fluid Power and Mechatronic Control Engineering, Atlantis Highlights in Engineering, Kunming, China, 7 December 2022.
183. Vignarooban, K.; Xu, X.; Arvay, A.; Hsu, K.; Kannan, A.M. Heat transfer fluids for concentrating solar power systems-a review. *Appl. Energy* **2015**, *146*, 383–396. [\[CrossRef\]](#)
184. Afzal, M.; Sharma, P. Design and computational analysis of a metal hydride hydrogen storage system with hexagonal honeycomb based heat transfer enhancements-part A. *Int. J. Hydrogen Energy* **2021**, *46*, 13116–13130. [\[CrossRef\]](#)
185. Afzal, M.; Sharma, P. Experimental analysis of a metal hydride hydrogen storage system with hexagonal honeycomb-based heat transfer enhancements-part B. *Int. J. Hydrogen Energy* **2021**, *46*, 13131–13141. [\[CrossRef\]](#)
186. Eisapour, A.H.; Eisapour, M.; Talebizadehsardari, P.; Walker, G. An innovative multi-zone configuration to enhance the charging process of magnesium based metal hydride hydrogen storage tank. *J. Energy Storage* **2021**, *36*, 102443. [\[CrossRef\]](#)
187. Raju, N.N.; Muthukumar, P.; Selvan, P.V.; Malleswararao, K. Design methodology and thermal modelling of industrial scale reactor for solid state hydrogen storage. *Int. J. Hydrogen Energy* **2019**, *44*, 20278–20292. [\[CrossRef\]](#)
188. Anbarasu, S.; Muthukumar, P.; Mishra, S.C. Tests on LmNi4. 91Sn0. 15 based solid state hydrogen storage device with embedded cooling tubesPart A: Absorption process. *Int. J. Hydrogen Energy* **2014**, *39*, 3342–3351. [\[CrossRef\]](#)
189. Anbarasu, S.; Muthukumar, P.; Mishra, S.C. Tests on LmNi4. 91Sn0. 15 based solid state hydrogen storage device with embedded cooling tubesPart B: Desorption process. *Int. J. Hydrogen Energy* **2014**, *39*, 4966–4972. [\[CrossRef\]](#)
190. Anbarasu, S.; Muthukumar, P.; Mishra, S.C. Thermal modeling of Mg₂Ni-based solid-state hydrogen storage reactor. *Heat Transf. Eng.* **2014**, *35*, 1354–1362. [\[CrossRef\]](#)
191. Schlichting, H. *Boundary Layer Theory*, 7th ed.; McGraw-Hill: New York, NY, USA, 1979.
192. Claman, M.; Minton, P. An experimental investigation of flow in an oscillating pipe. *J. Fluid Mech.* **1977**, *81*, 421–431. [\[CrossRef\]](#)
193. Lin, C.X.; Ebadian, M.A. Developing turbulent convective heat transfer in helical pipes. *Int. J. Heat Mass Transf.* **1997**, *40*, 3861–3873. [\[CrossRef\]](#)
194. Pendyala, R.; Jayanti, S.; Balakrishnan, A.R. Convective heat transfer in single-phase flow in vertical tube subjected to axial low frequency oscillations. *Heat Mass Transf.* **2008**, *44*, 857–864. [\[CrossRef\]](#)
195. Visaria, M.; Mudawar, I. Experimental investigation and theoretical modeling of dehydrating process in highpressure metal hydride hydrogen storage systems. *Int. J. Hydrogen Energy* **2012**, *37*, 5735–5749. [\[CrossRef\]](#)

196. Yang, F.S.; Zhang, Z.W.; Bao, Z.W. An extensive parametric analysis on the performance of a single-state metal hydride heat transformer. *Int. J. Hydrogen Energy* **2012**, *37*, 2623–2634. [CrossRef]
197. Yang, F.S.; Wang, G.X.; Zhang, Z.X.; Rudolph, V. Investigation on the influences of heat transfer enhancement measures in a thermally driven metal hydride heat pump. *Int. J. Hydrogen Energy* **2010**, *35*, 9725–9735. [CrossRef]
198. Malleswararao, K.; Aswin, S.; Murthy, S.S.; Dutta, P. Studies on a dynamically coupled multifunctional metal hydride thermal battery. *J. Alloy Compd.* **2021**, *866*, 158979. [CrossRef]
199. Mou, X.; Bao, Z.; Huang, W. Performance investigation of metal hydride reactor equipped with helically coiled heat exchanger during hydrogen absorption and desorption. *Therm. Sci. Eng. Prog.* **2023**, *38*, 101656. [CrossRef]
200. Afzal, M.; Mane, R.; Sharma, P. Heat transfer techniques in metal hydride hydrogen storage: A review. *Int. J. Hydrogen Energy* **2017**, *42*, 30661–30682. [CrossRef]
201. Jiao, K.; Li, X.; Yin, Y.; Zhou, Y.; Yu, S.; Du, Q. Effects of various operating conditions on the hydrogen absorption processes in a metal hydride tank. *Appl. Energy* **2012**, *94*, 257–269. [CrossRef]
202. Sandrock, G. *State-of-the Art Review of Hydrogen Storage in Reversible Metal Hydrides for Military Fuel Cell Applications*. Final Report Contract. 1997, pp. 1–159. Available online: <https://apps.dtic.mil/sti/citations/ADA328073> (accessed on 2 March 2025).
203. Klopčič, N.; Grimmer, I.; Winkler, F.; Sartory, M.; Trattner, A. A review on metal hydride materials for hydrogen storage. *J. Energy Storage* **2023**, *72*, 108456. [CrossRef]
204. Nuss, P.; Eckelman, M.J. Life cycle assessment of metals: A scientific synthesis. *PLoS ONE* **2014**, *9*, e101298. [CrossRef]
205. Liu, J.; Li, K.; Cheng, H.; Yan, K.; Wang, Y.; Liu, Y.; Jin, H.; Zheng, Z. New insights into the hydrogen storage performance degradation and Al functioning mechanism of LaNi_{5-x}Al_x alloys. *Int. J. Hydrogen Energy* **2017**, *42*, 24904–24914. [CrossRef]
206. Mirabile Gattia, D.; Montone, A.; Di Sarcina, I.; Nacucchi, M.; De Pascalis, F.; Re, M.; Pesce, E.; Vittori Antisari, M. On the degradation mechanisms of Mg hydride pellets for hydrogen storage in tanks. *Int. J. Hydrogen Energy* **2016**, *41*, 9834–9840. [CrossRef]
207. Dieterich, M.; Pohlmann, C.; Bürger, I.; Linder, M.; Röntzscher, L. Long-term cycle stability of metal hydride-graphite composites. *Int. J. Hydrogen Energy* **2015**, *40*, 16375–16382. [CrossRef]
208. Nemukula, E.; Mtshali, C.B.; Nemangwele, F. Metal hydrides for sustainable hydrogen storage: A review. *Int. J. Energy Res.* **2025**, *2025*, 6300225. [CrossRef]
209. Fadonougbo, J.O.; Kim, H.; Suh, B.; Yim, C.D.; Na, T.; Park, H.; Suh, J. On the long-term cyclic stability of near-eutectic Mg-Mg₂Ni alloys. *Int. J. Hydrogen Energy* **2022**, *47*, 3939–3947. [CrossRef]

Disclaimer/Publisher’s Note: The statements, opinions and data contained in all publications are solely those of the individual author(s) and contributor(s) and not of MDPI and/or the editor(s). MDPI and/or the editor(s) disclaim responsibility for any injury to people or property resulting from any ideas, methods, instructions or products referred to in the content.